CANMET

Canada Centre for Mineral and Energy Technology

Centre canadien de la technologie des minéraux et de l'énergie

REPORT 79-11

CANMET'S ROCK MECHANICS RESEARCH AT THE KIDD CREEK MINE

D.G.F. HEDLEY, G. HERGET, P. MILES AND Y.S. YU

MINERALS RESEARCH PROGRAM
MINING RESEARCH LABORATORIES

Energy, Mines and Resources Canada

Énergie, Mines et Ressources Canada

MAY 1979

Available in Canada through

Authorized Bookstore Agents
and other bookstores

or by mail from

Canadian Government Publishing Centre
Supply and Services Canada
Hull, Quebec, Canada K1A 0S9

CANMET
Energy, Mines and Resources Canada,
555 Booth St.,
Ottawa, Canada K1A 0G1

or through your bookseller.

Catalogue No. M38–13/79-11 Canada: $3.50
ISBN 0-660-10472-5 Other countries: $4.20

Price subject to change without notice.

En vente au Canada par l'entremise de nos

agents libraires agréés
et autres librairies

ou par la poste au:

Centre d'édition du gouvernement du Canada
Approvisionnements et Services Canada
Hull, Québec, Canada K1A 0S9

CANMET
Énergie, Mines et Ressources Canada,
555, rue Booth
Ottawa, Canada K1A 0G1

ou chez votre libraire.

Nº de catalogue M38–13/79-11 Canada $3.50
ISBN 0-660-10472-5 Hors Canada $4.20

Prix sujet à changement sans avis préalable.

CANMET'S ROCK MECHANICS RESEARCH AT THE KIDD CREEK MINE

by

D.G.F. Hedley*, G. Herget*, P. Miles**, and Y.S. Yu*

ABSTRACT

The Kidd Creek mine of Texasgulf Metals Company started as an open pit and later converted to an underground operation. In 1972, a cooperative rock mechanics research project was initiated between the company and the Mining Research Laboratories of CANMET. Research was concerned with stability of the hanging wall pit slope as it was undercut by the underground operations and with ground control aspects of the blasthole open stoping method employed underground.

Geotechnical investigations on critical joint orientations and shear resistance along these discontinuities indicated that a plane or rotational shear type of instability of the hanging wall slope was unlikely. This was confirmed by two- and three-dimensional finite element models, although sloughing of the hanging wall shear zone was predicted. Further confirmation on slope stability was obtained by monitoring slope displacement which showed a cause-and-effect relationship while mining was taking place and the magnitude was within the limits predicted from the two finite element models. During the time these studies were being done, stopes were being blasted through at the southern end while the pit was being deepened at the northern end. No instability of the pit walls interrupted either operation and the pit was completed in 1977.

Underground, field stress measurements were taken down to a depth of 850 m, indicating that the stress regime was similar to that in other mines in northern Ontario with horizontal stresses being greater than vertical stresses. Deformation measurement around underground stopes showed that expansion of the footwall shear zone was ten times greater than the pillar wall. There was a distinct cause-and-effect relationship between blasting and deformation. Pillar strength was estimated using a size/strength relationship, obtained from testing samples up to 25 cm in diameter, incorporated into an empirical strength equation. A preliminary analysis on pillar stability suggested that stresses on the pillar edge and corners could be of the same magnitude as pillar strength. This could explain the cases of pillar sloughing, but adverse structural geology could also have caused this sloughing.

Key words: Rock Mechanics, Open Pit, Open Stoping, Finite Element, Structural Geology, Surveying, Field Stresses, Borehole Extensometers, Slope Stability, Pillar Stability.

*Research Scientists, **Engineer, Mining Research Laboratories, CANMET, Energy, Mines and Resources Canada, Elliot Lake and Ottawa.

RECHERCHE SUR LA MECANIQUE DES ROCHES EFFECTUEE A LA MINE DE KIDD CREEK PAR CANMET

par

D.G.F. Hedley*, G. Herget*, P. Miles** et Y.S. Yu*

RESUME

La mine de Kidd Creek appartenant à la compagnie Texasgulf Metals a d'abord été exploitée à ciel ouvert pour être transformée en exploitation souterraine par la suite. En 1972, la compagnie et les Laboratoires de recherche minière de CANMET ont collaboré à l'élaboration d'un programme de recherche sur la mécanique des roches. La recherche était axée sur la stabilité de la lèvre supérieure de la pente d'une mine au moment de l'excavation souterraine et sur les aspects de la stabilité du terrain aux environs du trou de mine que l'on a excavée par la méthode d'exploitation à chambres ouvertes.

Les études géotechniques effectuées sur les orientations des joints critiques et la résistance au cisaillement le long de ces discontinuités démontrent qu'un type de cisaillement-plan ou rotatif de l'instabilité de la lèvre supérieure est invraisemblable. Cela a été confirmé à l'aide de modèles d'éléments fins à deux et à trois demensions quoique l'on avait prédit une séparation de la zone de cisaillement de la lèvre supérieure. En mesurant le déplacement dans la pente, on a pu confirmer les notions de stabilité de la pente qui démontrent qu'il y a un rapport cause à effet pendant l'exploitation et que la magnitude était entre les limites prévues à partir des deux modèles à éléments fins. Lorsque l'étude a été entreprise, les pentes du coté sud ont été abattues par le tir tandis que la fosse du côté nord a été creusée. Aucune instabilité des parois de la mine à ciel ouvert n'a interrompu ces deux opérations et la mine a été achevée en 1977.

Au sous-sol, on a mesuré les contraintes jusqu'à une profondeur de 850 m démontrant ainsi que le système des contraintes est semblable à celui des autres mines au nord de l'Ontario; les contraintes horizontales sont plus grandes que les contraintes verticales. La mesure de la déformation aux alentours des gradins souterrains a démontré que l'expansion de la zone de cisaillement de la lèvre supérieure est dix fois plus grande que les parois. Il y a un rapport cause à effet distinct entre le tir et la déformation qui en résulte. La résistance des piliers a été estimée à l'aide du rapport grosseur à résistance obtenu en analysant des échantillons pouvant aller jusqu'à 25 cm de diamètre et introduit dans une équation de résistance empirique. Une analyse préliminaire sur la stabilité des piliers a invoqué que les contraintes soumises aux bords et sur les coins du pilier pouvaient être de la même magnitude que la résistance du pilier. Ceci peut expliquer les cas de désagrégation des piliers mais une géologie structurale défavorable peut aussi en avoir été la cause.

Mots-clés: Mécanique des roches, exploitation à ciel ouvert, exploitation à chambres ouvertes, éléments fins, géologie structurale, levé, contraintes, extensomètres, stabilité de la pente, stabilité des piliers.

*Chercheurs scientifiques, **Ingénieur, Laboratoires de recherche minière, CANMET, Energie, Mines et Ressources Canada, Elliot Lake et Ottawa.

CONTENTS

TABLES

CONTENTS (cont'd)

FIGURES

CONTENTS (cont'd)

1. INTRODUCTION

In 1972, a cooperative research project was initiated between the Kidd Creek mine of Texasgulf Canada Limited and the Mining Research Laboratories of the Canada Centre for Mineral and Energy Technology. At that time the open pit was in operation and had progressed down to half its ultimate depth and the underground mine was being developed for production. The objectives of the joint project were:

a) to monitor and evaluate stability of the hanging wall slope of the open pit as it was undercut by underground stopes; and
b) to contribute to the design of the underground mining method by examining ground control aspects.

A number of monitoring and analytical studies were undertaken, some of which are still continuing. These included:

- monitoring movement of the hanging wall pit slope using an electro-optical surveying instrument;
- monitoring the rock deformation around the underground stopes with borehole extensometers;
- determining the strength of rock types in and surrounding the orebody;
- measuring the field stresses down to 850 m using overcoring techniques;
- estimating the stresses and deformations produced by underground mining by two- and three-dimensional (2-D and 3-D) finite element (FE) models; and
- determining the structural geological features and properties of the hanging wall pit slope using conventional direct mapping and photogrammetric techniques.

In all, twelve internal reports have been written describing these studies. This report combines all these studies into one report describing the measuring techniques and their applications, comparing measured and predicted deformations and stresses, and evaluating potential modes of failure.

By 1978 the open pit mine had been completed. Several stopes had been blasted through into the bottom of the pit undercutting the hanging wall slope. This has resulted in no visual deterioration of the pit wall although displacements up to 9 cm have been measured. Some 20 stopes have been mined by blasthole open stoping, several of which have been backfilled with cemented rockfill. A number of problems have arisen with sloughing of the pillars and of the hanging wall and footwall shear zones. The mine staff is consequently examining modifications to the method as the mine is deepened.

2. MINING BACKGROUND

The mine is located within the city limits of Timmins in northern Ontario. Massive sulphide copper-zinc orebodies, which also contain lead, silver, cadmium and tin, are associated with a steeply-dipping rhyolitic pile intersected by numerous shear zones (1). In general, the orebodies have an overall north-northeast strike and dip 70 to 80° east. Maximum length is 670 m, maximum width is 170 m, and the deposit is known to extend beyond 1500 m in depth.

The open pit started in 1965 and operated for twelve years, producing about 30 million tonnes of ore. It is in the shape of a tear-drop with the apex to the south. Surface dimensions are 820 m long by 490 m wide and the depth varies from 100 m at the south end to 230 m at the north end. Bench intervals are 12 m with a 12-m wide safety berm left at every second bench. Overall slope angle is about 50°, although at the shallower southern end the slope angle is about 56°. Access is by two ramps on the east and west sides, which join on the north wall (2).

Sinking of a 930-m deep shaft commenced in 1969 and at the same time an inclined ramp was driven from the second bench on the west wall down to the 1200 level (3). Sinking of a second shaft started in 1974 down to a planned depth of 1615 m. The underground mine is developed by levels at 122-m intervals starting at 244 m (800 level) with sub-levels at 30.5-m intervals (4). A blasthole open stoping method is used to mine 18-m wide transverse stopes and 25-m wide pillars. Stope length between hanging wall and footwall

varies up to 75 m and stope height is 80 m, leaving a 26-m crown pillar between stoping blocks (4). However, crown pillars are not left between the open pit and the stopes immediately below it, and several stopes have been blasted through into the pit. It is intended to bulk-fill the stopes with cemented rockfill prior to mining the pillars.

Figure 2.1 is a generalized longitudinal section through the open pit and underground mine showing the progress of mining up to early 1978. Production from the stopes started in 1973 and about 7 million tonnes of ore had been mined up to the end of 1977. Present mining is mostly confined to the 800 and 1200 level stopes with development being done on the 1600, 2000 and 2400 levels.

3. OPEN PIT INVESTIGATIONS

Instability of a pit slope usually occurs in one of three modes: plane shear, rotational shear, and block flow and toppling as illustrated in Fig. 3.1, 3.2 and 3.3 (5).

Plane shear instability is the most common form in hardrock slopes and occurs when discontinuities are unfavourably oriented and the shear strength on these discontinuities is insufficient to prevent sliding.

Where the orientation of the discontinuities is not critical and in more ductile material such as overburden, instability can occur by rotational shear. In this case the shear strength of the intact rock is overcome and sliding takes place on a circular surface.

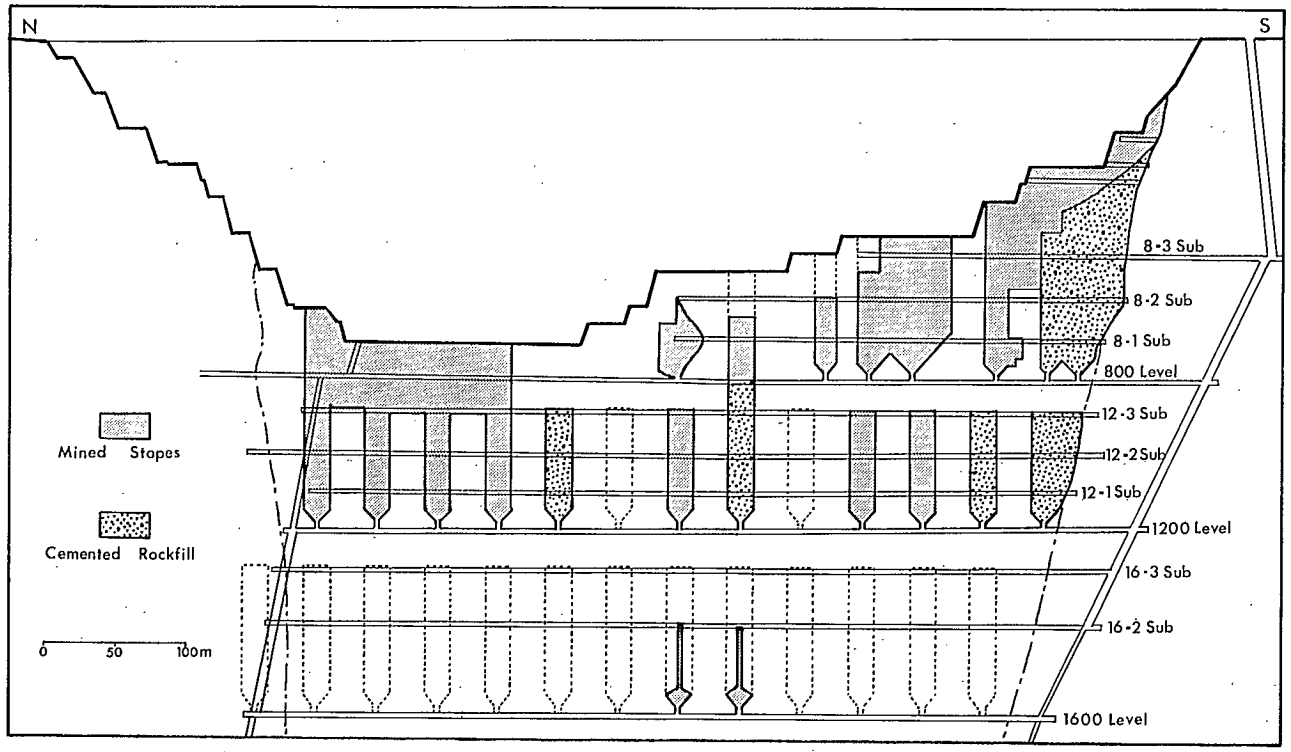

Fig. 2.1 - North-South longitudinal section through orebodies

Block flow and toppling modes of instability are possible in brittle rocks when the stress concentration at the toe of the slope exceeds the compressive strength, resulting in crushing.

To evaluate the possibility of these modes of instability occurring requires geotechnical information. Surveys were made, measurements taken and testing done to determine rock properties, surface and near-surface structural features, groundwater, and rock permeability. Finite element models were constructed to predict redistribution of stresses and resultant displacements caused by underground mining. A comprehensive remote monitoring system was installed to measure absolute displacement of the southeast pit slope to provide a warning system and identify any mode of instability that developed.

These studies were concentrated on the southeast hanging wall slope which was to be the first section undercut by underground mining.

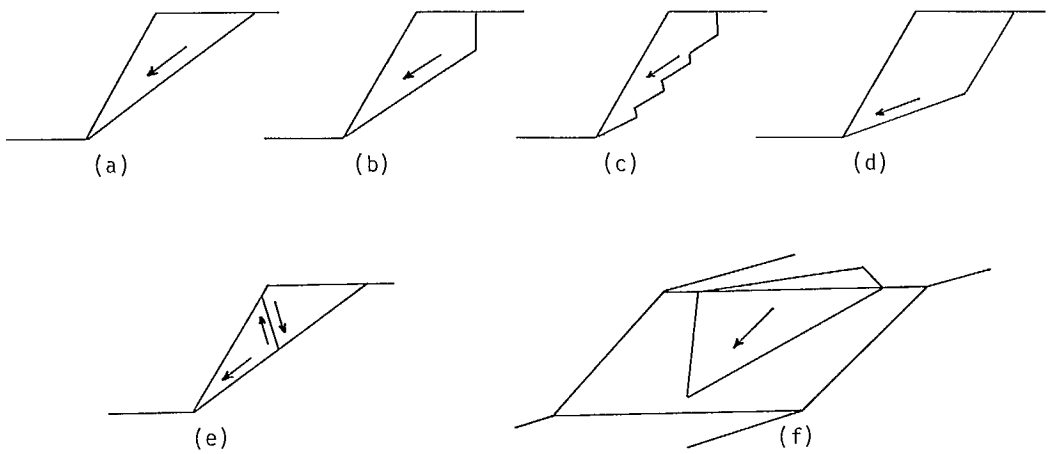

Fig. 3.1 - Plane shear instability modes: (a) one sliding plane and one block; (b) one sliding plane and a tension crack; (c) a series of short sliding planes with connecting cross joints; (d) two sliding planes; (e) a single sliding plane with the sliding block shearing into several blocks; and (f) two oblique sliding planes and a 3-D wedge.

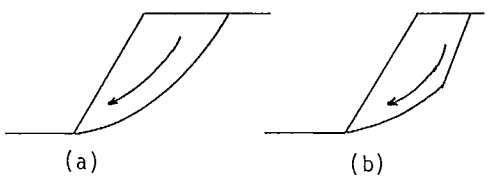

Fig. 3.2 - Rotational shear. In ductile rock without critically oriented planes of weakness, the potential mode of instability would be by rotational shear as shown in (a). This sometimes occurs in combination with a sliding plane as shown in (b).

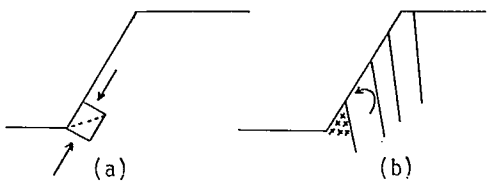

Fig. 3.3 - Block flow and toppling. In brittle rock without a critically oriented plane of weakness, instability would be initiated by crushing or shearing at the toe of the slope as indicated in (a) possibly leading to block flow and toppling of slabs represented by (b).

3.1. ROCK PROPERTIES

A typical transverse section at the southern end of the open pit is shown in Fig. 3.4 illustrating the rock types and faulting in this area. Compressive strength and deformation characteristics were determined for each rock type which from east to west are:

1. hanging wall andesite/diorite
2. serquanite (rhyolite, pale green chert)
3. hanging wall shear zone with basic dikes of andesite/diorite
4. massive sulphide ore
5. footwall shear zone with rhyolite

5a footwall rhyolite with tuff (no shearing)

6. footwall andesite/diorite

The andesite/diorite in the hanging wall and footwall were judged similar so that only samples from the hanging wall were considered. Sampling in the pit was impractical and rock samples were obtained by drilling from underground development headings regarded as being representative of the rock types. Various sizes of samples were taken to obtain an indication of the effect of sample size on strength.

All samples were cut at a length to diameter ratio of 2:1 and the parallelism achieved between ends of the rock cylinders was within 0.1% of the sample diameter. Axial deformation to calculate elastic modulus and total strain up to failure was obtained by mounting three LVDT units on the specimen so that deformation was monitored between the specimen ends. All samples were loaded to failure in one cycle and elastic moduli were calculated at 50% of the compressive strength. A total of 140 samples of sound rock were tested for which the average results are given in Table 3.1.

Compressive strength varied with sample diameter; there was an increase in strength between 32 mm and 41 mm in diameter, then a consistent decrease to 245 mm. Using the 41-mm diameter samples as a standard, the andesite/diorite was the strongest rock with not much difference shown between the ore, serquanite, and non-sheared footwall rhyolite. The hanging wall shear zone had a strength about 75% that of the ore and the footwall shear zone was the weakest rock with a strength about 33% of the ore.

No large difference in elastic moduli was observed in relation to either rock strength or sample size and a common value of $E = 80 \times 10^3$ MPa appeared to be adequate for most rock types, except for the footwall shear zone where the elastic modulus was 50×10^3 MPa.

3.2. STRUCTURAL GEOLOGY

Major faults in the southern end of the open pit are shown in Fig. 3.5. Faults in the southeast or pit area dip steeply. In the extreme south end of the pit the Ancillary Shear and the North-South Shear appear to coincide to form a zone of strong schistosity dipping approximately 70-80° to the east. The underground extent of these two major shears is shown in Fig. 3.4. A correlation between underground levels indicates that the Ancillary Shear remains in the hanging wall having a dip varying from 55 to 80° east. Between 800 level and 8-3 sub-level, the strike of the Ancillary Shear changes to approximately true east-west with dips varying from 75° south at 800 level to 55° south at 8-3 sublevel. Surface mapping has identified a branch of the Ancillary, which changes strike also to approximately true east-west with a dip of 85° north. If a correlation exists between these east-west trending shear zones, the shear plane could provide one side for a major rock wedge in the southeast corner of the pit.

Orientations of joint sets and minor shears were measured by line mapping along the haulage ramp and No. 8 bench. In addition, terrestrial photogrammetry was used to determine orientations of geological discontinuities (6). A phototheodolite was located on a base line on the opposite northwest slope and stereo photographs taken of the southeast pit wall.

Contoured, equal area plots of the poles of these structural features using both measuring techniques are shown in Fig. 3.6 (a) and (b). There was close agreement between the two methods. Maximum difference in the dip direction was 17° for joint set C and 11° difference in dip angle for joint set A. In general, line mapping is preferred to photogrammetry as the measurements

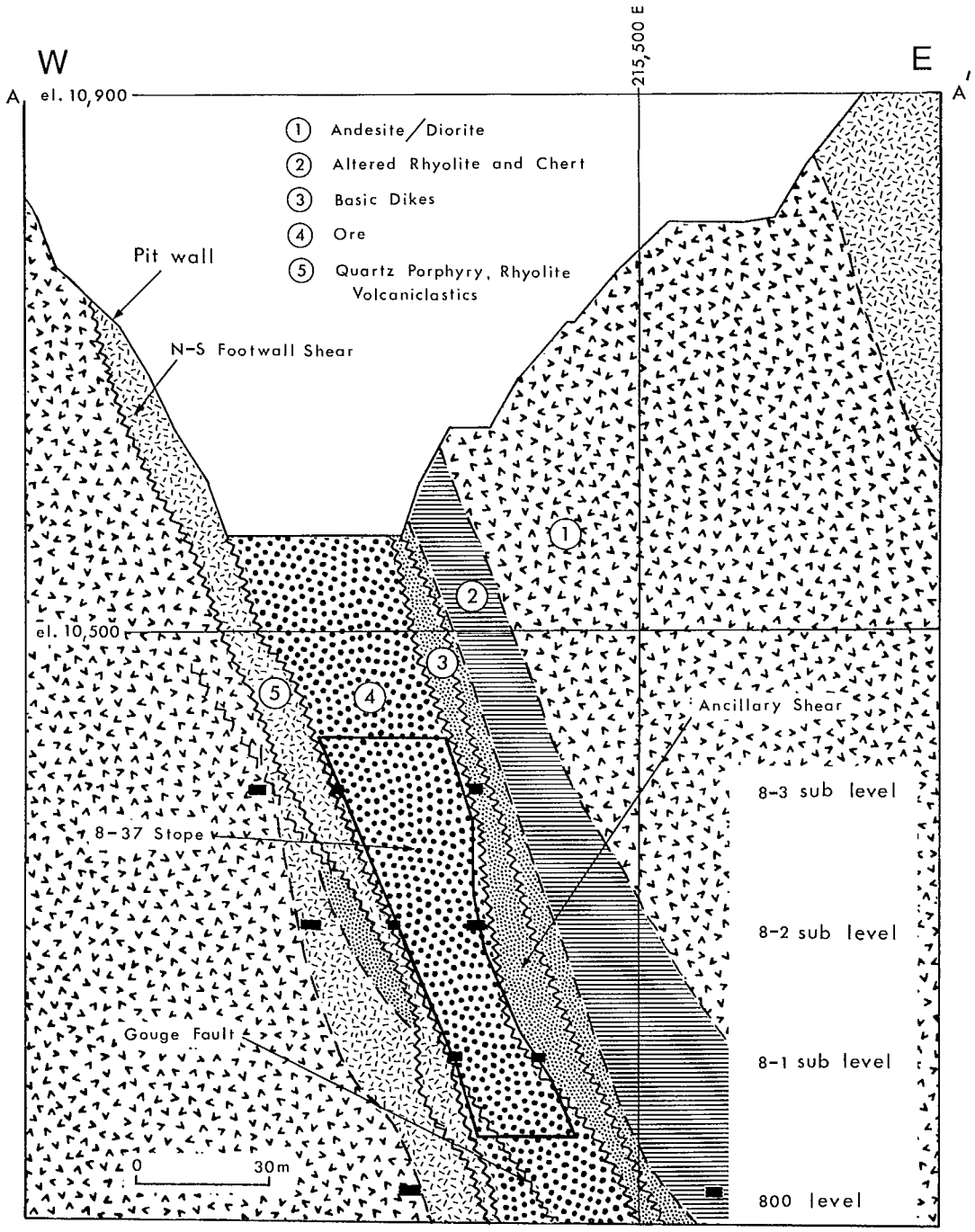

Fig. 3.4 - East-west geological section through southern end of open pit

Table 3.1 - Uniaxial compression tests on drill core

Rock type	Density (kg/m³)	Core diam. (mm)	Compressive strength (MPa)	Elastic modulus (1000 MPa)	Poisson's ratio	No. of specimens
			Mean ± Std. Dev.	Mean ± Std. Dev.	Mean ± Std. Dev.	
1) Andesite/ diorite	2960	32	158 ± 75	94 ± 29		9
		41	202 ± 53	82 ± 7		10
		72	163 ± 64	85 ± 8		10
		245	120 ± 47	81 ± 7	0.23 ± 0.01	3
2) Serquanite	2700	32	87 ± 23	77 ± 14		14
		41	147 ± 37	81 ± 2		10
		72	119 ± 17	82 ± 3		12
		245	82 ± 13	73 ± 3	0.14 ± 0.01	3
3) H/W shear zone (andesite/diorite)	2850	41	117 ± 53	81 ± 8		8
4) Ore	3330	32	132 ± 73	81 ± 13		10
		41	159 ± 27	73 ± 12		13
		72	144 ± 36	78 ± 7		13
		245	149 ± 28	83 ± 3	0.21 ± 0.05	3
5) F/W shear zone (rhyolite)	2750	41	53 ± 17	50 ± 17		10
5a) F/W rhyolite + tuff	2700	41	167 ± 58	74 ± 14		12
						140

are direct and the results and analysis are available in less time. Photogrammetry should be considered when larger properties are investigated and accessibility is a problem.

In terms of slope stability, joints of set A which are dipping into the pit at an angle of 30° could provide a sliding plane. Joints and shears of sets B and C could provide the boundaries of a rock wedge. These stability aspects are examined later.

3.3. SHEAR RESISTANCE OF DISCONTINUITY SURFACES

Five 245 mm-diam samples and 18 smaller samples containing geological discontinuities were used to determine shear resistance under triaxial conditions. Surface appearance allowed a threefold grouping of the discontinuity surfaces:

1. clean, rough (joints)
2. dark coloured, slickensided, rough (shears)
3. dark coloured, slickensided, smooth (shears).

Orientation of the discontinuities varied between 25° and 75° to the long axis of the sample and slip tests were carried out in seven stages with a variation of the confining pressure between 0.2 MPa and 6.6 MPa which resulted in a range of normal stresses on the geological discontinuities from 0.6 to about 55.2 MPa.

In a triaxial slip test the confining pressure, σ_3, is held constant and the axial stress, σ_1, in the specimen is increased until slippage occurs. For this point the normal, σ_n, and shear stresses, τ, can be calculated according to inclination, α, of the discontinuity to the axis of the specimen. Corrections for the friction occurring along one specimen end were taken into account. The coefficient of friction, μ, is then calculated from the ratio τ/σ_n. Sliding does not occur when $\mu > \cot \alpha$. This was observed in ten cases where α ranged between 54° and 75° and as a result considerable fracturing occurred in the rock sample. Both the rough but clean and slickensided rough surfaces showed the limiting α angle to be about 54° to 55°. For the smooth slickensided surfaces, normal slippage occurred for a sample with α = 60° and only minor cracking was observed for a sample with α = 68°.

For the samples showing slippage, τ and σ_n were calculated and plotted in Fig.

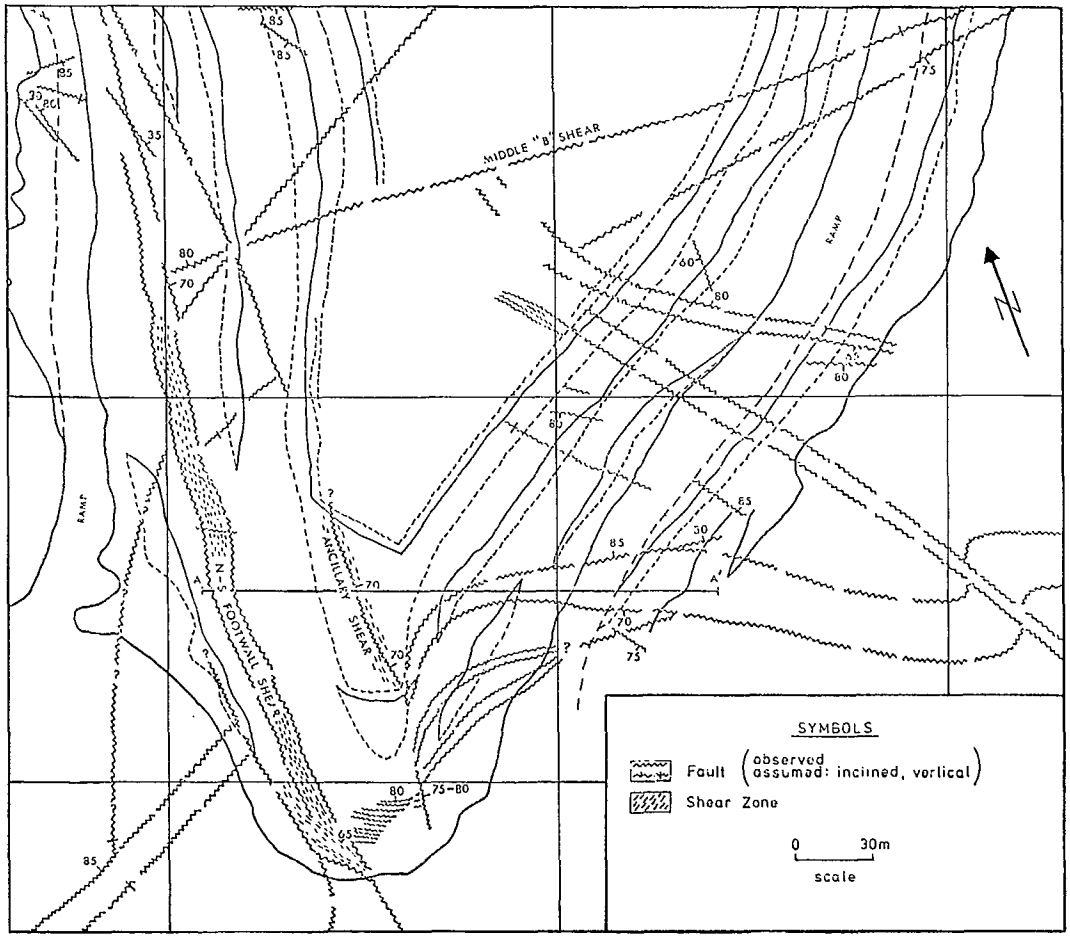

Fig. 3.5 - Pit contours and major faults in southern end of open pit

3.7. The plots showed that in most cases all points could be approximated by a straight line.

Even the first slip, X, which could be considerably higher in shear resistance due to breaking in of the shear surface, is located on the straight line. Wear of the discontinuities due to repeated slips is apparently negligible because only the last slip, or in two cases the last two slips showed a deviation from the straight line relationship. All but one sample showed a clear shear stress intercept and for these sample data the shear resistance is best described by:

$$\tau = C + \mu\sigma_n$$

C can be called cohesion, but it has to be understood that it derives from the interlocking of two matching fracture surfaces.

All observations close to the straight line were subjected to a linear regression analysis and μ and C were obtained. Results are listed in Table 3.2 by sample number and are grouped according to the type of geological discontinuity.

The results showed that differences in the coefficients of friction are rather insignificant compared with the large differences in discontinuity appearance. More significant are the differences in the shear stress intercepts which clearly set apart the three different

Maximum	Orientation (dip dir. /dip)
A	291°/30°
B	138°/90°
C	009°/83°

(Dip dir. given from true north)

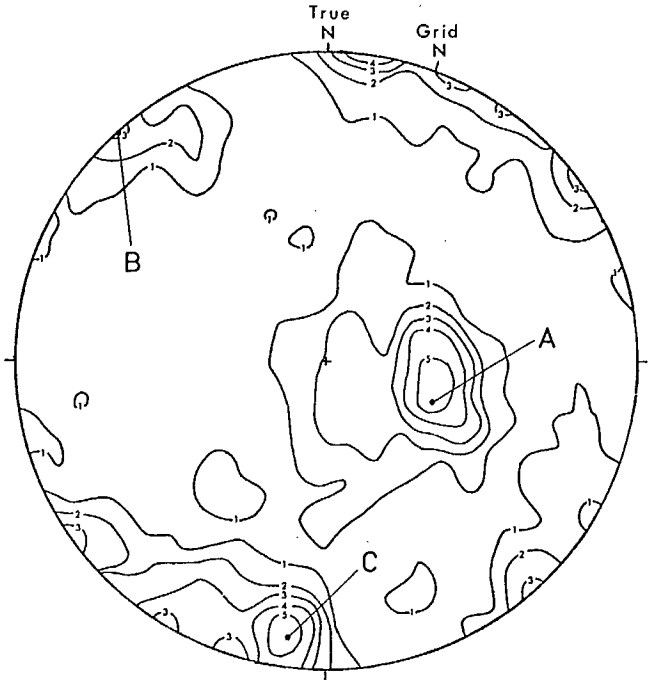

Fig. 3.6(a) - Contoured equal area net of 406 joints and shears in southeast slope using line mapping

Maximum	Orientation (dip dir. /dip)
A	291°/41°
B	142°/90°
C	352°/84°

(Dip dir. given from true north)

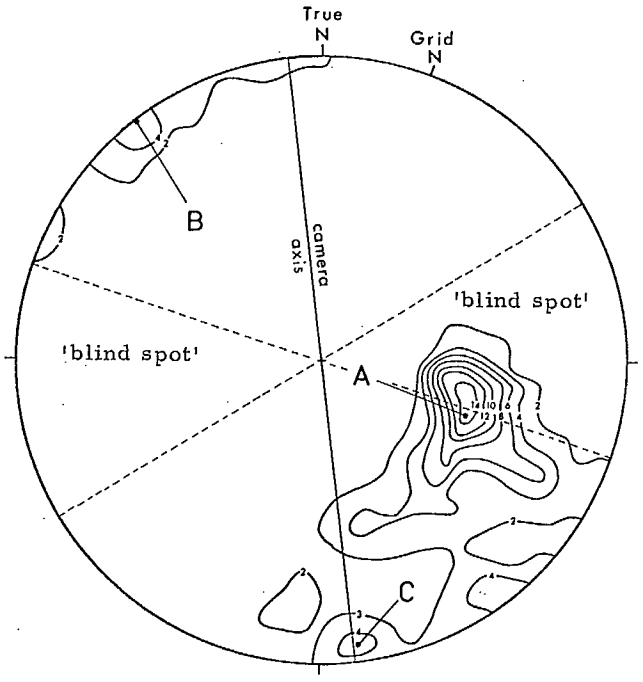

Fig. 3.6(b) - Contoured equal area net of 122 joint planes in southeast slope using photogrammetric analysis

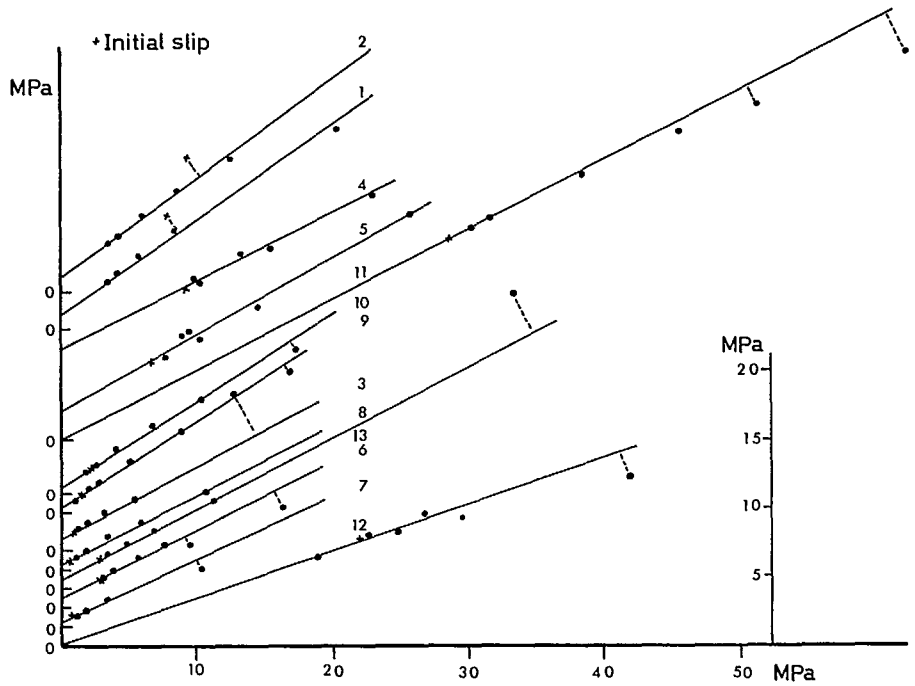

Fig. 3.7 - Shear stress against normal stress from triaxial tests on fracture surfaces

Table 3.2 - Mean values of coefficient of friction (μ) and shear stress intercept (C)

Sample No.	Discontinuity type	Rock type	μ	C (MPa)
3	rough,	ore	0.54	0.90
4	geological	andesite	0.51	4.00
5	fractures	basic dike	0.56	2.14
9		andesite	0.65	0.35
			0.57 ± 0.06	1.84 ± 1.62
1	rough,	andesite	0.74	1.03
2	slickensided	rhyolite	0.71	1.07
7	geological	rhyolite	0.45	0.35
8	fractures	andesite	0.50	0.41
			0.60 ± 0.15	0.72 ± 0.39
6	smooth	serquanite	0.50	0.69
10	slickensided	andesite	0.64	0.55
11	geological	rhyolite	0.50	0.00
12	fractures	rhyolite	0.34	0.00
13		rhyolite	0.52	0.69
			0.50 ± 0.11	0.39 ± 0.36

groups of discontinuities by surface roughness. Thus, for the description of shear resistance, in any preliminary design, it is suggested that a common coefficient of friction of $\mu = 55 \pm 0.11$ with separate shear stress intercepts, C, to be used according to the type of geological discontinuity.

3.4. GROUNDWATER AND PERMEABILITY

In the fall of 1973, piezometers were installed in two boreholes in the southeast corner of the pit to monitor groundwater levels and rock permeability.

Hole P1 had a diameter of 89 mm and was drilled from the crest of the pit to a depth of 61 m. Piezometers were installed at depths of 19.8, 45.7, and 61 m. Measurements in hole P1 made three months after installation, indicated no water in any of the piezometer standpipes.

Hole P2, 248 mm in diameter, was collared on the pit floor 97 m below the pit crest and drilled to a depth of 25.6 m. One piezometer was installed at a depth of 24 m. The water level, measured three and five months after the piezometer installation, was 12.5 m and 13.9 m respectively below the collar of the hole.

Observations of water seepage in the southeast slope at the time of the piezometer installations showed the face to be dry down to approximately 24 m below the bottom of hole P1. This would account for the absence of water in the P1 standpipes. Seepage from the southeast face was noticed at approximately 24 m above the water level found in hole P2. Because of the available drainage into the pit and underground workings, no adverse water pressures affecting slope stability were anticipated.

The coefficient of permeability, K, was calculated from falling head tests in saturated ground according to the following formula (7):

$$K = \frac{A}{F(t_2 - t_1)} \ln \frac{H_1}{H_2}$$

where: A = cross sectional area of water column,

H_1 = excess static head at time t_1,

H_2 = excess static head at time t_2,

F = test section shape factor for hole P2:

$$F = \frac{2L}{\ln (\frac{2L}{D})}$$

where: $L > 4D$

L = length of test section

D = borehole diameter

Permeabilities of 9.8×10^{-6} cm/s and 3.5×10^{-6} cm/s were calculated from falling head tests in hole P2 for September and November 1973 respectively. Figure 3.8 shows details of the falling head test carried out in hole P2 in September 1973. These permeability values are typical for tight, relatively impermeable formations.

3.5. GEOTECHNICAL EVALUATION OF SLOPE STABILITY

During the pit excavation and conversion from open pit to underground mining, three significant excavation stages could be distinguished for which slope stability assessments would be required:

(a) the slope below the haul road when the final pit floor is reached;

(b) the hanging wall of empty 838 stope below the haul road;

(c) long term stability of hanging wall above rock-filled 838 stope.

The stages are shown in Fig. 3.9 (a), (b) and (c) and their stability was evaluated for potential instability modes, safety factor and probability of instability (5).

Figure 3.4 provides a geological cross section and Fig. 3.6(a) indicates the distribution of joints in the southeast wall of the pit. Deep seated rotational shear failure can be ruled out because of the high rock strength and the lack of ubiquitous fracturation.

Figure 3.6(a) can be typified by the three joint sets, A, B and C. Set A has a true mean strike of N 012E and a 30° dip into the pit and sets B and C display a nearly vertical dip and strikes of N 048°E and N 098E. This configuration

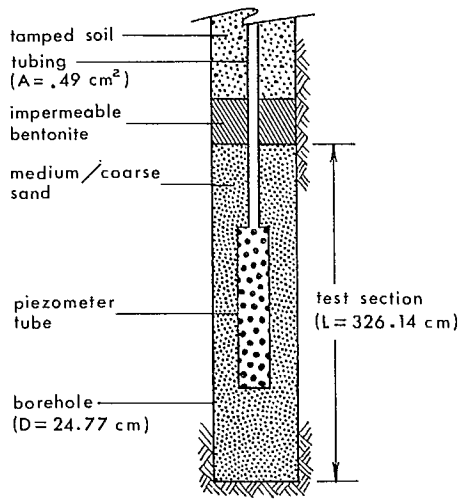

Piezometer Installation in Hole P2

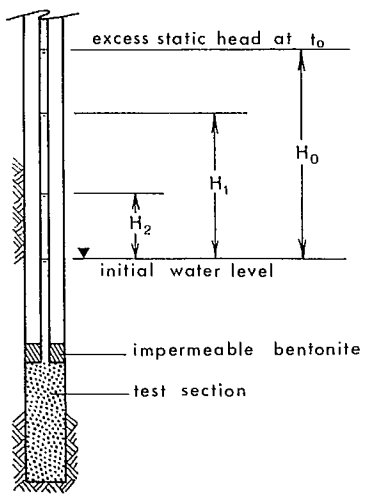

Falling Head Test

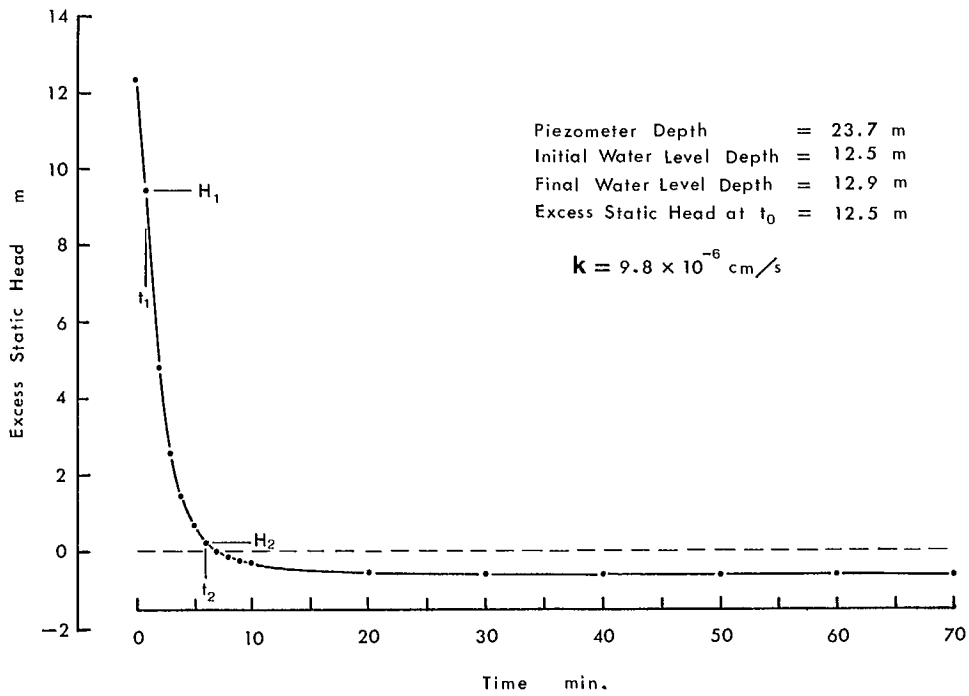

Fig. 3.8 - Falling head test in hole P2 (Sept. 1973)

practically excludes the possibility of block flow occurring, but will encourage backbreak to vertical faces and requires an assessment of whether set A could cause plane shear failure.

Stage (a) concerns the slope from below the haul road to the pit floor (Fig. 3.9a). The average slope angle is 50°, the height is 72 m and the line intersecting the toe of the slope and the east side of the haul road has a dip of 40°. The slope can be considered to be fully drained. Previously the shear resistance has been described by:

$$\tau = C + \sigma_n \tan \phi$$

with ϕ being 28.8° and C varying between 0.39 MPa for slickensided smooth geological fractures and 1.84 MPa for rough geological fractures. Taking the lower cohesion value and an average rock density of 2900 kg/m^3 an apparent angle of friction, ϕa, of 70.9° represents the total mobilized shear resistance.

$$\phi_a = \text{arc tan } (\frac{\tau}{\sigma_n}) = \text{arc tan } \left(\frac{C + \sigma_n \tan \phi}{\sigma_n} \right)$$

This apparent angle of friction exceeds the mean slope angle and, considering that the chances of finding a continuous geological fracture at a dip of 40° are small, the slope is considered stable.

Stage(b) concerns the stability of the overhang above the empty 838 stope (Fig. 3.9b). This overhang above the floor of the stope is 170 m high at an angle of 71°. Apart from the most likely unravelling of the ancillary shear in the hanging wall of the stope, the greatest likelihood of instability seems to be a vertical failure surface developing along existing geological fractures in the hanging wall of the 838 stope. As the stope was going to be filled soon after ore removal, only short-term stability is required.

The cohesion value for the rough geological fractures would hold the overhang in place, but the lower cohesion value of 0.39 MPa would not provide adequate strength. This unstable condition is, however, based on the assumption that a relatively smooth geological fracture exists in a strike parallel to the hanging wall and with a 90° dip extending from the hanging wall side of the stope floor to the intersection of the pit slope below the haul road. It also requires that release fractures exist on the north and south sides of the stope to allow outward movement of such a slab.

Figure 3.6(a) shows that nearly vertical fractures exist approximately parallel and at right angles to the stope (Sets B and C). Field mapping has indicated, however, that the required continuity of 170 m is not present and that considerable material bridges and interlocking asperities have to be crushed to interconnect the existing intermittent geological fractures for failure to occur. Assuming that material bridges occupy 5% of the 170 m long potential failure surface and possess a shear strength of one fifth of the uniaxial compressive strength, the overhang is stable (8). In addition, the release fractures north and south of the stope will provide wedging action due to waviness and hold the overhang in place for a short time. A word of caution is necessary, however, because with time, material bridges and interlocking asperities in the shear surfaces will deteriorate due to blasting action and climatic effects and will result in future instability of the large overhang.

Stage (c) involves the hanging wall slope above the backfilled stope (Fig. 3.9 c) and below the haul road. This slope has a face angle of 50°, an overhang of 71°, and a height of 103 m. Connecting the toe of the slope with the east side of the haul road, the failure surface would have an inclination of 54°. Based on a cohesion of 0.39 MPa for the failure surface, a friction angle of ϕ = 28.8°, and a rock density of 2900 kg/m^3 above the failure surface, the apparent angle of friction σ_a, would be 58°. Joint set A which has a dip component into the pit, is shown with intervals of 0.5 standard deviation around the mean of the joint cluster A in Fig. 3.10 (9,10). Drawing a friction circle of 58° shows that it embraces three standard deviations of the cluster mean, and considering that neither the assumed low cohesion values nor the 100% con-

tinuity are likely to exist for a large failure surface, instability is unlikely.

The overhang of 12 m with a height of 55 m above the top of the rock fill has to be regarded in a similar way as the stage (b) overhang and has to be considered unstable for the long term.

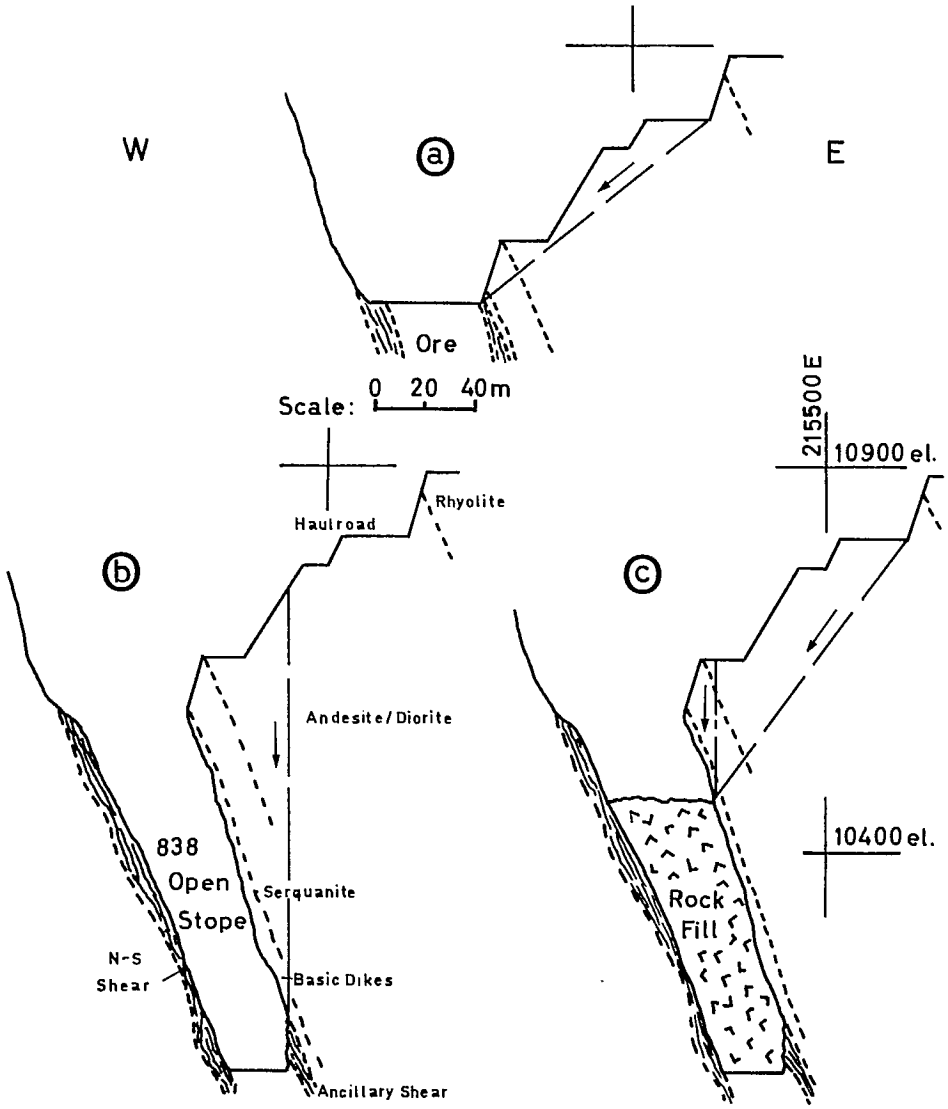

Fig. 3.9 - Significant excavation stages for hanging wall: (a) final pit slope, (b) overhang of 838 stope and (c) stope above 838 stope with cemented rock fill.

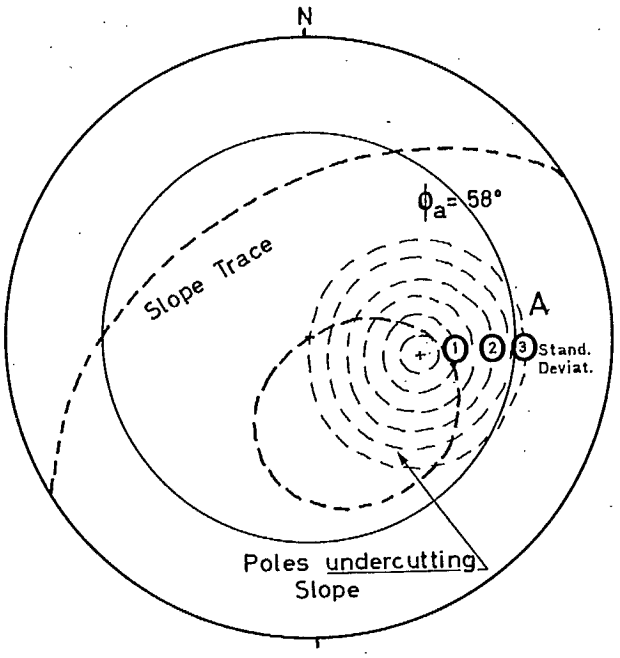

Fig. 3.10 - Lower equal area net showing joint set A with multiples of 0.5 standard deviation about the mean and the 58° apparent friction circle

3.6. FINITE ELEMENT MODELS

The stability of mine structures depends primarily on how the rock behaves under stresses around the excavations as mining progresses. Therefore, some knowledge of stress distribution in and around the pit wall is a fundamental requirement for understanding pit wall behaviour. Knowledge of this kind provided some insight into the reactions of the southeast slope wall as it was undercut by stoping operations.

Stresses and displacements in an open pit mine can be approximated by using 2-D plane strain or axisymmetric solutions. In some instances, however, a 3-D analysis is required for more realistic idealization. When several stopes and crown pillars have been mined through into the open pit at the south end of the Kidd Creek mine, its geometry is really three dimensional. It was realized that a 2-D model which simulates an open pit of this kind, naturally was not adequate. But the cost of conducting 3-D FE analysis was high even for a relatively small-scale model, thus 3-D modelling for the Kidd Creek mine was considered impracticable at the time when the project was initiated. To provide some preliminary information on stresses and displacements, etc., around the mine, 2-D plane strain models were first constructed and investigated for a variety of geometries and loading conditions.

During 1976 an effort was made at the Mining Research Laboratories, to reduce computer costs for the 3-D stress analysis using the SAP3D program by optimizing the stiffness assembly routine and the equation-solving routine. Program efficiency was greatly improved resulting in a substantial reduction in computer costs. Consequently a 3-D FE model of moderate size of a portion of the mine was constructed and examined for the same loading conditions.

3.6.1. Mine Model and Extraction Sequence

A typical section from the southern end of the pit, where the southeast pit wall is undercut by stoping operations, is shown in Fig. 3.11(a). The distribution of rock types is also shown. Although the FE modelling technique is capable of handling a complex structure and geology, cost makes it essential to simplify the geology and the geometry. The idealized geology for this section is shown in Fig. 3.11(b). The rock mass consists of five different types of rocks numbered 1 to 5 for material identification.

As the FE method can handle only finite regions and most mine structures are essentially infinite, it is necessary to truncate the actual structure. A compromise has to be made between introducing a large model with correspondingly higher computer costs or a small model with relatively larger errors in the calculated displacements and stresses. Some limited theoretical results and testing with progressively larger models leads to the conclusion that, in general, fictitious outer boundaries placed at a distance of four or five times the size of the excavation should limit these errors to about 10% or less. This accuracy is adequate for most engineering applications.

The design of the Kidd Creek mine model, either 2-D or 3-D, follows this criterion. The section simulated by the FE model in plane strain

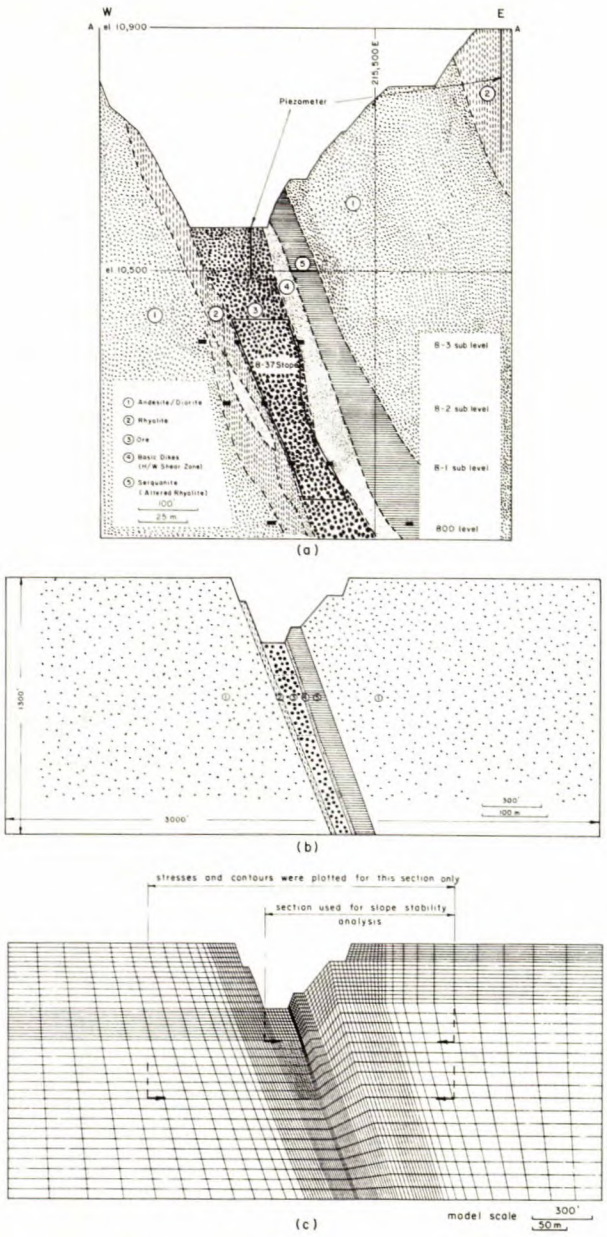

Fig. 3.11 - Two-dimensional FE model: (a) general geological features, (b) simplified geology and geometry, (c) FE mesh.

is 400 m vertically and 915 m wide. The mesh network of the FE model is shown in Fig. 3.11(c); only quadrilateral elements were used. The total number of elements was 2531 and of nodes, 2656. The bottom of the mine model was fixed in the y or vertical direction whereas the sides were constrained in the x or horizontal direction for simulation of boundary conditions.

Similarly full-scale 3-D modelling for the Kidd Creek mine was not possible at this stage and a compromise had to be made. Therefore, only a block or slice of the open pit at the south end was considered and simulated.

A model 168 m thick along the long axis of the pit, 915 m wide and 400 m high was constructed. This was based on the profile of section 3750S, the same section used for the 2-D simulation. This model consists of two 18.3-m wide by 91.5-m high stopes separated by a 24.4-m pillar; the crown pillars above the stopes were also mined out. For simplicity it was assumed that variation of the pit geometry in the x-direction, i.e., along the long axis of the pit remained the same. Therefore, only one half of the model needed to be considered. A perspective view of this mode is shown in Fig. 3.12(a) and the plane view in Fig. 3.12(b) which shows that the block was further divided into six slices or seven sections with thicknesses varying from 9 to 20.5 m. As an example, only one cross section with finite element mesh of the 3-D model is shown in Fig. 3.12(c). Two adjacent plane sections form one 3-D solid slice which yields 521 eight-node brick elements and 580 nodes. Thus the model has a total of 3126 elements and 4060 nodes with a maximum half-band-width of 398.

Mining operations usually involve a sequential excavation. Thus it is important to study the change of stresses of displacements in the mine structures from one mining stage to another. Analytical simulation procedures have been developed and incorporated into the FE analysis making it possible to simulate a proposed sequence of mining.

Three mining stages were examined in the 2-D simulations; Stage I was the open pit without underground stope development. Subsequently the effect of excavating the underground stope was simulated by removing the dotted elements in Fig. 3.11(c); this is referred to as Stage II. In Stage III, an additional effect of removing the crown pillar between the pit bottom and the stope was simulated. Stresses and excavation displacements were determined for each stage. Also slope stability was evaluated using the Mohr-Coulomb criteria.

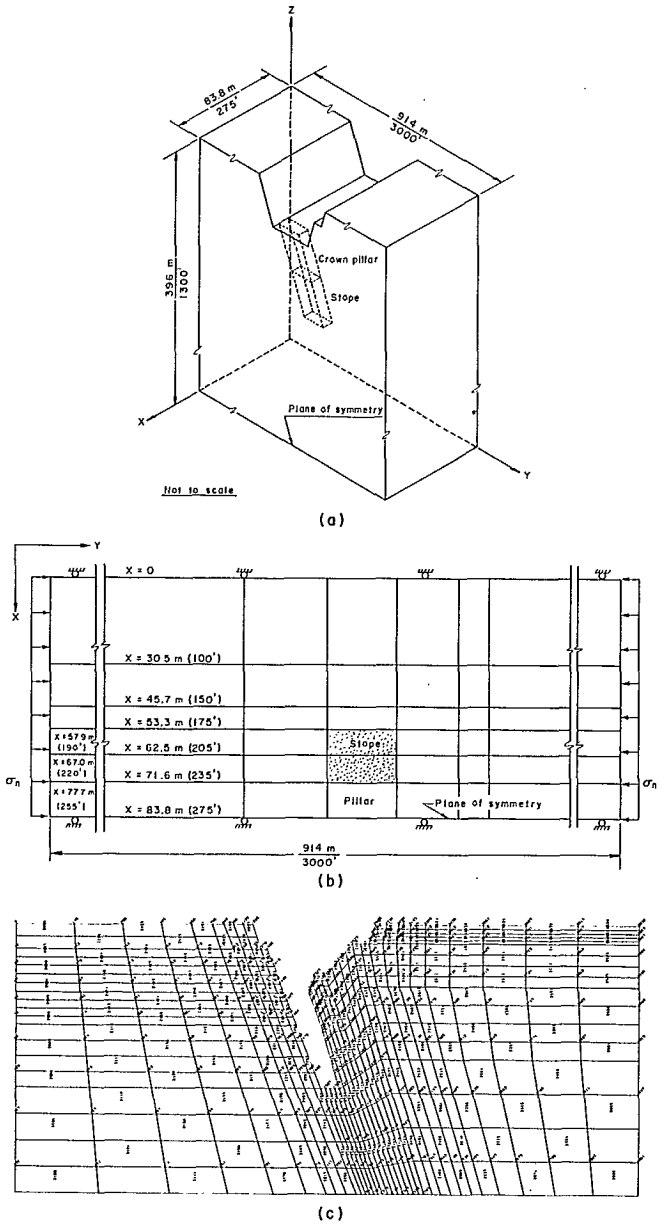

Fig. 3.12 - Three-dimensional FE model: (a) perspective view and definition of axes, (b) plan view, (c) FE mesh for section x = 62.5 m.

For the 3-D simulation, only Stage III with two mined-out stopes and their crown pillars was examined. Stresses and excavation displacement were also determined for this model and slope stability was evaluated using the Drucker/Prager yielding criteria.

3.6.2. Physical Properties and Field Stresses

The modulus of deformation, E, Poisson's ratio, ν, and the unit weight, γ, for the mine rocks as shown in Table 3.3 were determined in the laboratory by testing small rock samples as described in section 3.1. It is recognized that the modulus of deformation of the rock substance is usually higher than that of the rock mass. Reduction factors based on a modified core recovery, designated as RQD (rock quality designation) have been applied (11). An empirical equation has been deduced to estimate the modulus of deformation of a rock mass, E_{rm}, from that of the intact rock substance E_s:

$$E_{rm} = (4.5\ RQD - 3.05)E_s \quad \text{for RQD} > 70\% \qquad \text{Eq 1}$$

$$E_{rm} = 0.1\ E_s \quad \text{for RQD} < 70\% \qquad \text{Eq 2}$$

By applying the above equations, the in situ moduli for the mine rocks were estimated based on limited RQD information available at the time when the models were constructed. The modified values contained in Table 3.3 were used in the analysis.

No large differences in Poisson's ratio were observed in relation to rock types, therefore, a value of 0.20 apeared to be adequate. The other material properties of the mine rocks required for subsequent stability analysis were the shear strength parameters, C and ϕ. A regression analysis, based on the triaxial testing of drill cores containing geological fractures yielded average values of 1.73 kPa and 29°, respectively, for C and ϕ. These appeared to be the lower bound of the shear strength parameters for the rock mass when the joints or fractures were critically oriented. In other words, the cohesive strength of the rock mass should be much greater than that of the fractures. An estimate of 5.17 kPa and 34° for C and ϕ respectively would be reasonable for the types of rock involved.

When the initial finite element models were constructed, the magnitude of the vertical and horizontal field stresses were unknown. Three stress regimes were tested covering the

Table 3.3 - Physical properties of mine rocks for finite element analysis

Code No.	Rock type	Estimated RQD %	Modulus of deformation (1000 MPa) Laboratory	Modulus of deformation (1000 MPa) In situ	Poisson's ratio Laboratory	Poisson's ratio In situ
1	Andesite/diorite	82	87	57	.23	.20
2	Rhyolite (Footwall shear zone)	50	50	5		.20
3	Ore	83	78	54	.20	.20
4	Basic dikes (hanging wall shear zone)	50	81	8		.20
5	Serquanite	72	80	15		.20

range from only gravitational stress to tectonic horizontal stresses as follows:

Case A: $\sigma h = K\gamma Z$, $\sigma z = \gamma Z$

Case B: $\sigma = 7928 + K\gamma z$, $\sigma z = \gamma Z$

Case C: $\sigma h = 7928 + 41.6z$ $\sigma z = \gamma Z$

where σh and σz are the horizontal and vertical stresses in MPa, γ is the unit weight of rock, z is the depth below surface in metres, K is a constant depending on Poisson's ratio, ν, and equals $\nu/1-\nu$.

Subsequently, stress measurements at the mine, described in section 4.1, indicated that the field stresses were in agreement with Case C. Consequently, only the results for this tectonic loading condition are described in this section.

3.6.3. Two-Dimensional Model

The stress trajectories and contours of principal stresses for the three stages of mining are presented in Fig. 3.13, 3.14 and 3.15. Compressive stresses around the toe of the pit before stoping were approximately 30.0 to 34.5 MPa and increased to about 40.0 when the stopes were mined in Stage 2. Similarly, high stress concentrations were located around the upper corners of the stope with a maximum of about 48.0 MPa. When the crown pillar was removed in Stage 3, these compressive stresses were shifted and concentrated around the lower corners and floor of the stope.

Tensile zones up to 6.2 MPa were evident in the upper part of the stope hanging wall during Stage 2. Under such conditions, local instability would be expected and minor sloughing from the stope walls had occurred in the stopes. On removal of the crown pillar in Stage 3, the tensile zone extended to a large part of the hanging wall and the upper part of the footwall. Tensile stresses of 4.8 MPa were indicated near the bottom of the stope, 2.8 MPa at the toe haulage ramp and 0.7 MPa along the footwall surface behind the crest which is not evident in conditions at the minesite. In the 2-D model removing the crown pillars is equivalent to mining an infinitely long trench and the stresses have to be redistributed around the bottom of the stope. In the actual 3-D condition, transverse pillars between stopes would allow the stresses to be transferred laterally as well as vertically. Hence the stresses developed in the 2-D model would be much more severe than those expected in situ.

As the stress field in the pit slope has been determined from the 2-D FE model, the normal and shear stresses acting at points along any potential failure surface may be found using an interpolation procedure. The potential failure surface, in this case, is usually approximated by a number of segments or chords with equal length and the stresses are calculated at the centre of each segment or chord. With the normal and shear stresses known, the resisting strength can be found from the Mohr-Coulomb equation. From the mechanics of limiting equilibrium, the factor of safety may be evaluated as the ratio of resisting

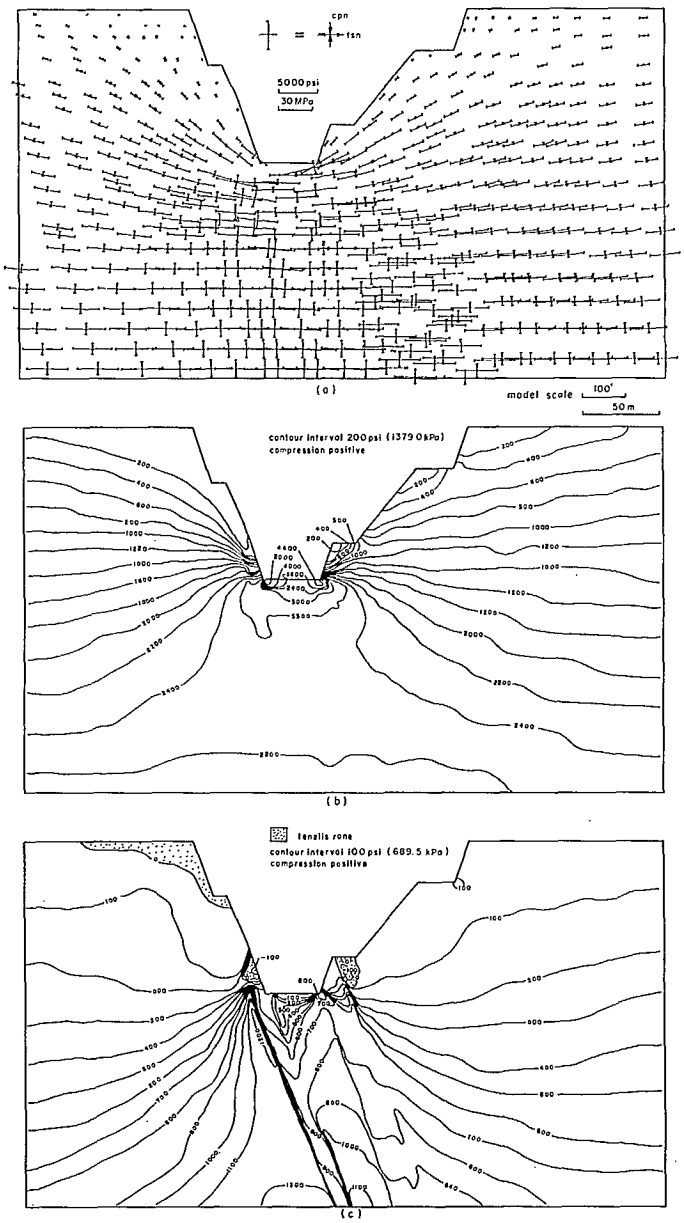

Fig. 3.13 - Stress distribution in 2-D model after stage I: (a) stress trajectories, (b) major principal stresses, (c) minor principal stresses.

strength to the total shear force along any potential failure surface. The total shear resistance (strength) and the total shear forces can be determined by summing the shear resistance and shear force at all the points (centre of each chord) along the potential failure surface. The factor of safety is determined by:

$$FS = \frac{S(C + s_n \tan d)\, dl}{S t_m dl}$$

in which s_n and t_m are the components of normal and shear stresses, respectively, with respect to the tangent to the failure surface and dl is an incremental length.

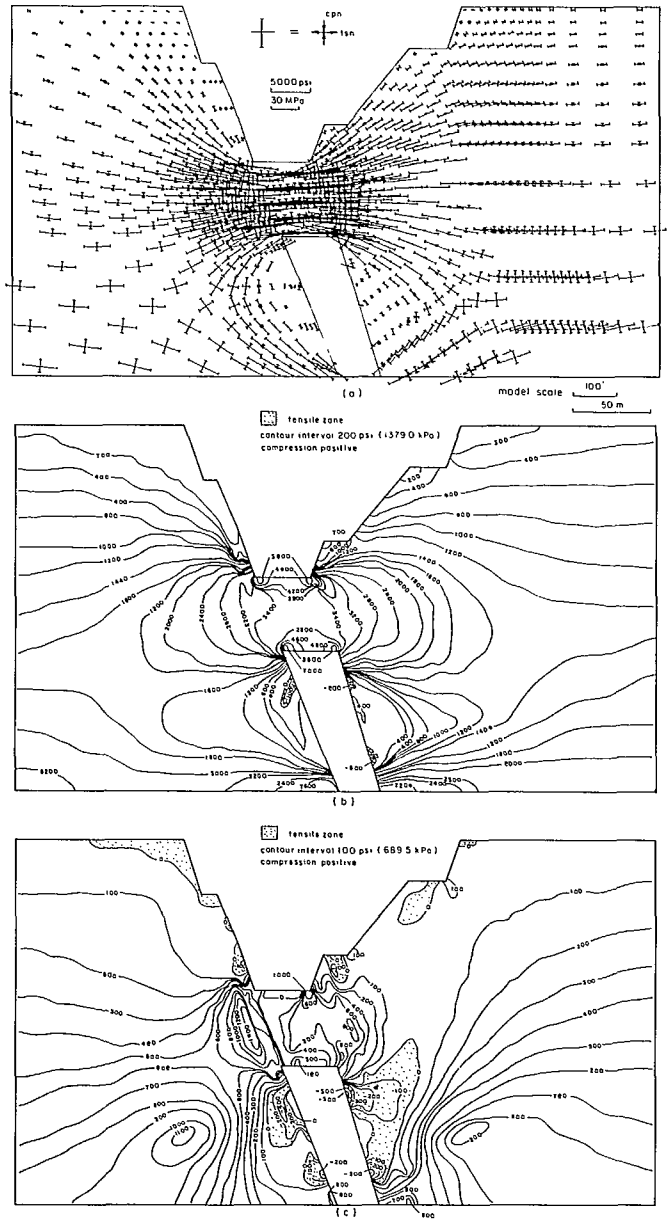

Fig. 3.14 - Stress distribution in 2-D model after stage II: (a) stress trajectories, (b) major principal stresses, (c) minor principal stresses.

This analysis involves a procedure of successive trials (12). A potential failure surface is chosen and the factor of safety against sliding along that surface is determined. Different potential surfaces are selected and the analysis is repeated until the potential failure surface having the lowest factor of safety is found.

A region of the SE slope wall as shown in Fig. 3.11(c) was selected for the analyses. Some "worst possible" conditions were assumed, i.e., low shear strength parameters, with C varying from 0.34 MPa to 1.38 MPa and d varying from 29° to 34°, were assumed. Pore pressure was not included in these analyses because the rock appeared to be dry above the 160 m elevation.

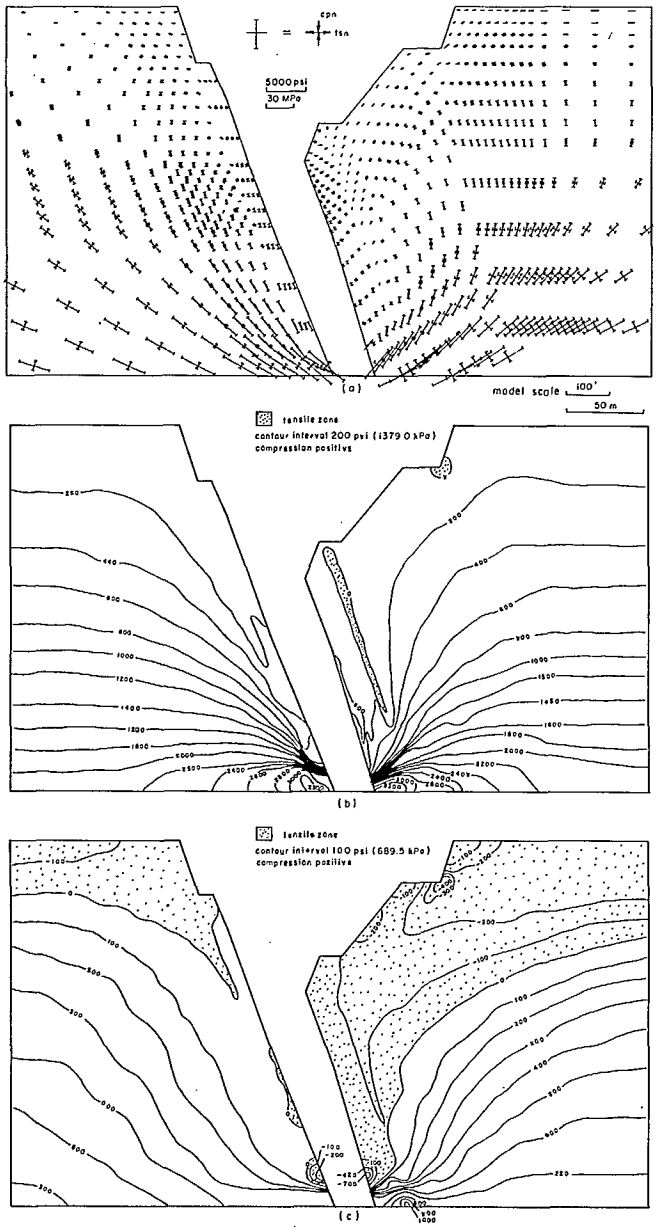

Fig. 3.15 - Stress distribution in 2-D model after stage III: (a) stress trajectories, (b) major principal stresses, (c) minor principal stresses.

Therefore, the exclusion of pore pressure will not affect the applicability of the result significantly. A number of trials were carried out; results indicated that neither rotational shear failure, circular and non-circular, nor plane shear failure were likely to occur under the assumed loading and plane strain conditions.

3.6.4. Three-Dimensional Model

The principal stress contours resulting from mining the open pit plus two stopes with an intervening pillar are presented in Fig. 3.16 and 3.17 respectively for section x = 67.0 m through the stope and x =77.7 m through the pillar. The highest concentrations of compressive stress are

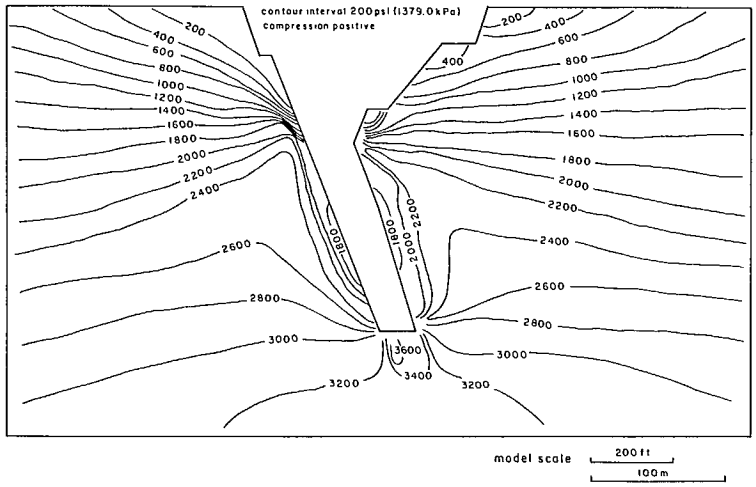

(a)

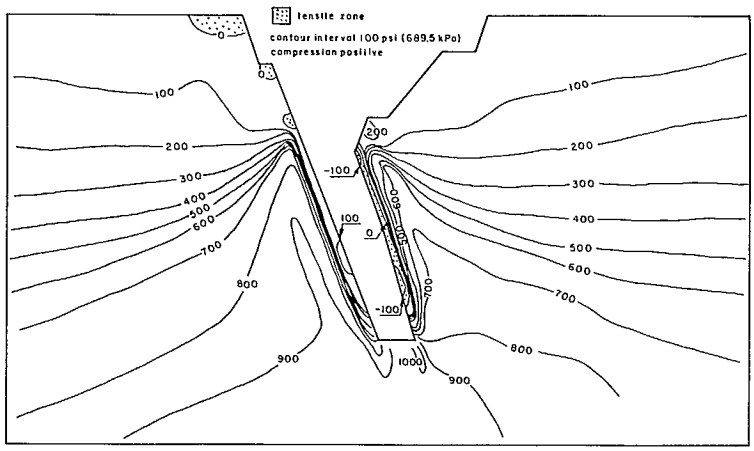

(b)

Fig. 3.16 - Three-dimensional stress distribution for section x = 67.0 m: (a) major principal stresses, (b) minor principal stresses.

at the top of the pillar at about 45.5 MPa and at the floor of the stope at about 25.0 MPa. In general, these stresses are lower and more evenly distributed than in the comparable 2-D case (Fig. 3.15), as the stresses can be transferred laterally to the centre pillar and side abutments as well as vertically.

The tensile zone is considerably reduced and is essentially confined to the hanging wall shear zone. This is more in keeping with visual observations in the open pit where no tensile cracks are evident and in the underground stope where sloughing of the shear zone occurs.

Rock displacements resulting from mining both the open pit and two stopes are shown in Fig. 3.18 for the two sections. For comparison the displacements from the 2-D model are also shown. In general, displacements in the 3-D model are almost horizontal. Maximum displacement of the hanging wall at the centre of the stope is about 4.2 cm compared with about 9.0 cm in the 2-D model, which is also more inclined downward.

Displacements in the footwall are very small in the 3-D model except for the shear zone where 4.5 cm is indicated. This large discontinuity of displacement probably was due to the mod-

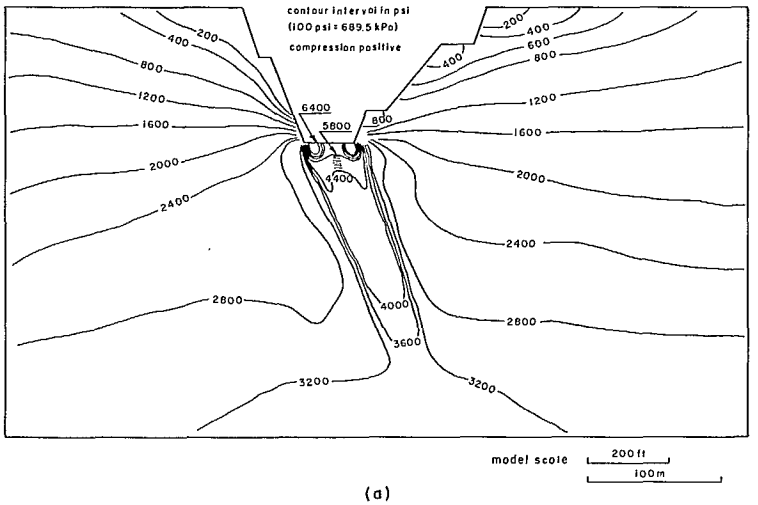

Fig. 3.17 - Three-dimensional stress distribution for section x = 77.7 m: (a) major principal stresses, (b) minor principal stresses.

ulus ratio (8.2 : 0.7) between the shear zone and footwall rock. In the 2-D case, displacement of the shear zone was about 7.5 cm.

Slope stability for the 3-D model can be analyzed in terms of the Drucker/Prager yield criteria.

The yield function is written:

$$F = \alpha I_1 + \sqrt{J_2} = k$$

where I_1 = first invariant of stress tensor

$$= (\sigma_x + \sigma_y + \sigma_z) = (\sigma_1 + \sigma_2 + \sigma_3)$$

J_2 = second invariant of the deviatoric stress tensor

$$= \frac{1}{6}\left[(\sigma_x - \sigma_y)^2 + (\sigma_y - \sigma_z)^2 + (\sigma_z - \sigma_x)^2\right] + (\tau_{xy}^2 + \tau_{yz}^2 + \tau_{zx}^2)$$

α = material constant

$$= 2 \sin\phi / [\sqrt{3}\,(3 - \sin\phi)]$$

k = material constant

$$= 6\, c \cos\phi / [\sqrt{3}\,(3 - \sin\phi)]$$

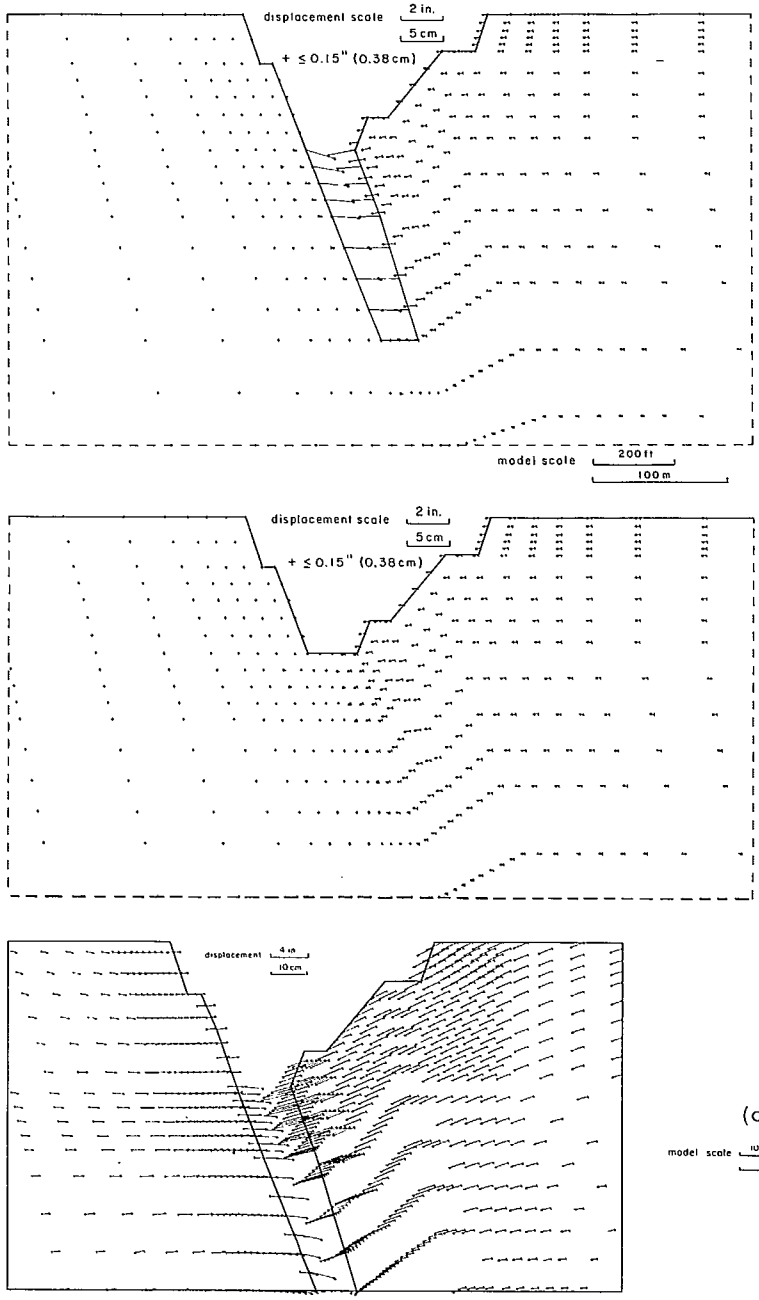

(a)

(b)

(c)

Fig. 3.18 - Excavation displacements: (a) 3-D model section x = 67.0 m, (b) 3-D model section x = 77.7 m, (c) 2-D model.

When the stresses in each element are known from 3-D FE model, the factor of safety FS in terms of I_1, J_2 and the material constants can be derived as:

$$FS = \frac{k - \alpha I_1}{\sqrt{J_2}}$$

An element becomes plastic or yielding when FS < 1.0 and FS > 1.0 indicates elastic behaviour.

Factors of safety in terms of the Drucker Prager yield stress function were calculated for the two sections and shown in Fig. 3.19. Material constants were assumed to be C = 0.69 MPa and

ϕ = 34° for the footwall and hanging wall shear zones and C = 5.17 MPa, ϕ = 34° for the rest of the rock mass.

Yield zones are indicated in the footwall and hanging wall shear zones in the stope and also along the edge of the pillar contact with the shear zones. This could lead to instability in the underground stopes and pillars in the form of sloughing in both the immediate hanging wall and footwall as well as the sides of the pillar. These yield zones will cause a further redistribution of stress which cannot be analyzed at the present stage. In comparison, the safety factors of both the hanging wall and footwall pit slopes are above 2.0 and should be stable for the geometries analyzed.

3.6.5. Discussion of Finite Element Results

It was not easy to select an adequate 2-D model to simulate an open pit mine of this kind as the geometry is really 3-D. Plane strain solutions can be used in some instances to approximate stresses and displacements in an open pit mine, and in other instances, a 3-D analysis is required for more realistic idealization of field conditions. However, knowledge of actual field conditions such as in situ physical properties, rock type distributions and the state of initial stresses, etc., remain a problem for both 2- and 3-D analyses. In spite of this difficulty and realizing the fact that the solutions are approximate, the results provide some insight into the reactions of the pit wall and around the stopes.

Two-dimensional FE analysis provided a fairly good approximation of stresses and displacement resulting from the first two stages of mining operations for the model, i.e., open pit mining (Stage I) and underground stoping (Stage II). However, when the crown pillar was extracted (Stage III) the 3-D model is considered more accurate and realistic.

In the 2-D simulation, mining of the open pit alone at the south end of the mine did not create stresses which were high enough to cause any instability around the pit walls. Slope stability analysis based on the FE stresses indicated that neither rotational shear, circular and non-circular, nor plane shear failure was likely to occur. Field observations in the past seemed to agree with this evaluation. With the stoping operation being completed (Stage II) the stress patterns were disturbed considerably with high stresses up to 48.2 MPa concentrated around the upper corner of the stope. Considering the high strength of ore, this stress condition should not pose any threat to instability. However, because of tensions developed around the stope walls, slabbing or sloughing should occur in that area and this seemed to be consistent with field observations.

Under 3-D simulation, tensions with a maximum of about 1.38 MPa were developed around the stope. This tension zone spread in both directions along the hanging wall and footwall as well as penetrating into pillars and abutment. Yield analysis indicated that minor shear fracture should occur along the stope walls. Furthermore, some local instability could be expected from the pillars between the excavated stopes.

The excavation displacements induced by undercutting from 2- and 3-D models were respectively directed approximately 30° downward and more than 30° horizontally into the pit. The largest magnitude of displacement along the SE pit wall was 9.0 cm from the 2-D model and 4.2 cm from the 3-D model. These calculated displacements are compared with measured displacements in section 3.7. It was also noted that the mining of stopes and crown pillars at the south end of the pit produced little effect on the footwall. In other words only minor deformation of less than 3 mm has developed except along the footwall shear zone. This large displacement presumably resulted from straining of the footwall shear zone due to high modulus ratio (8.10:0.72) between andesite/diorite and the footwall rock. However, these models are for elastic and continuous ground; structural discontinuities such as joints modify these movement patterns. The general effect of having a discontinuous mass is to add large components of downward and inward movements. From the view of stability, these deformations might be significant because they result in loosening

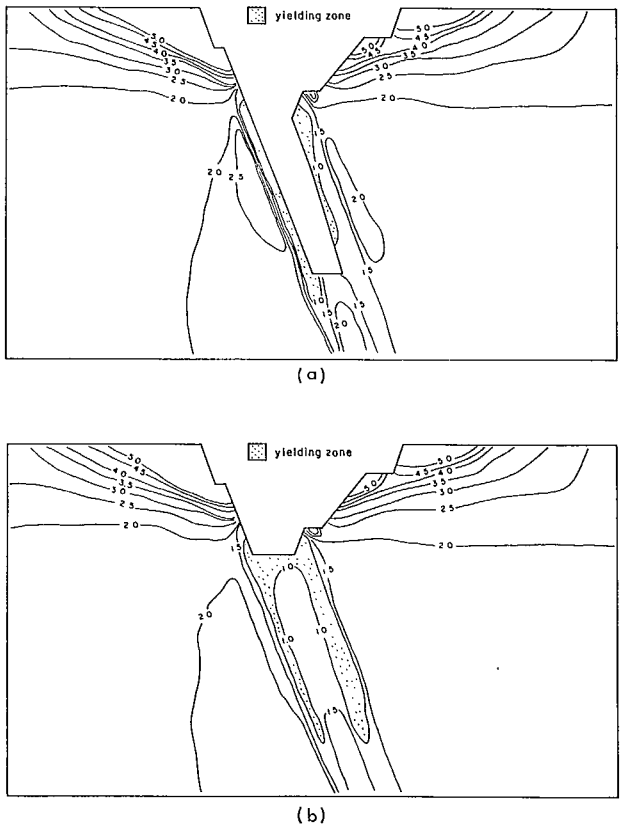

Fig. 3.19 - Local safety factor contours in terms of Ducker/Prager yielding criterion: (a) section x = 67.0 m, (b) section x = 77.7 m.

of the rock mass; hence movement of walls when mining out the ore would be worth measuring to provide a basis for predicting the onset of instability.

As mining progresses to a greater depth, an increase of stresses around the stope and in the pillars at a lower level would be expected. As more data on the physical properties of the rock mass and field stress conditions will be collected, a refined 3-D FE model should provide additional information which would be useful for mine design considerations at deeper levels.

3.7. OPEN PIT DISPLACEMENT MEASUREMENTS

One of the objectives of the cooperative study was to monitor the movement of the southeast pit slope as it was undercut by the underground stopes. Due to limited access to this part of the pit wall, a remote measuring system was required with targets permanently attached to the pit wall. Another restriction was that only one suitable location existed on the opposite side of the pit with clear lines of sight to the whole southeast pit wall. This required an instrument capable of measuring both distances and angles, and a Geodimeter 700 was chosen. In 1975 the company expanded the monitoring system to the west and north walls and purchased its own instrument, a later version Geodimeter 710.

The Geodimeter 700 and 710 measures the slope distance between the instrument and a glass prism reflector located on the pit wall by means of a laser beam. A distance to 1 mm is automatically displayed on a digital readout. Horizontal and vertical angles are also measured electronically to within a few seconds of arc and displayed on the same readout unit. Knowing the slope distance, vertical angle and horizontal angle from a known reference point, allows the 3-D coordinates of a glass prism target to be calculated.

3.7.1. Layout of Measurements

Figure 3.20 shows the configuration of the open pit and the locations of the instrument stations, reference stations and glass prism targets. In 1973, 30 targets were installed on the southeast pit wall and in 1976 a further 6 targets on the northeast pit wall. For measurements to these targets the Geodimeter was set up on the West Ramp Station with Outcrop East being used as a backsight and Outcrop South as a reference point. To obtain accurate measurements, it is essential that the reference stations do not move and it would have been preferable to locate these two stations further away from the open pit. However, they were the only two rock outcrops within several kilometres of the minesite.

In 1975/76 the company installed a further 20 targets on the west wall. Measurements to these targets are made with the Geodimeter set up on the Outcrop East Station and a three-prism target mounted on the concrete headframe is used as a backsight.

The construction details of the instrument stations and targets, measurement procedure,

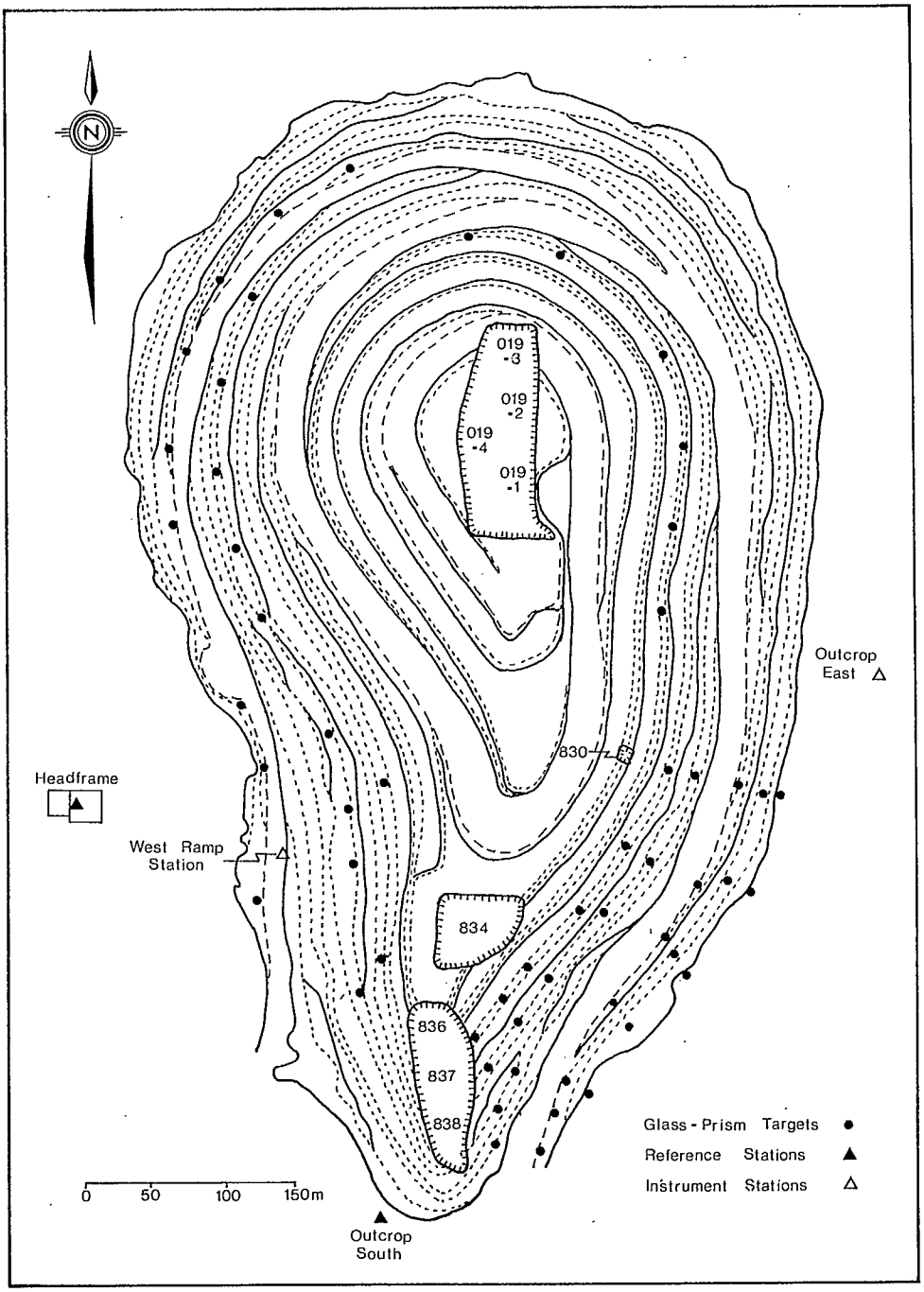

Fig. 3.20 - Layout of remote monitoring systems in the open pit

and a method of correcting the measurements are described in Appendix A. The latter was necessary due to the movement of the West Ramp Station which was located on the edge of the pit in fractured ground. Measurements to Outcrop East and Outcrop South allowed the calculation of this movement which amounted to 37 mm towards the pit in a northeasterly direction over a five-year period. In addition, periodic checks were made by triangulation between the three stations.

Sets of measurements were taken on a monthly basis by the surveying staff at the mine. Readings were originally taken only over the summer months, but with construction of huts

around the two instrument stations, monitoring has since extended over the winter months. However, some targets are covered by snow and measurements cannot be made. Over a five year period about 5000 sets of measurements have been taken.

3.7.2. Displacement of the Southeast Pit Wall

Figure 3.21 illustrates the total cumulative displacement since 1973 of the southeast pit wall to the end of the years 1975 through to 1978. The status of stopes broken through into the pit is also illustrated in these diagrams.

By the end of 1975, the 838 stope and pillar had been blasted through into the pit. The hanging wall shear zone in this area which is about 4 m thick sloughed into the stope. An initial breakthrough was also made on the 834 stope. Displacement, as shown in Fig. 3.21(a), indicates the southern end and the lower benches had moved 2 - 4 cm. The northern area and a tongue along the ramp had a displacement of less than 2 cm.

By the end of 1976 the 837 stope had been blasted and together with the 838 stope this opening had been backfilled with a crushed rock-cement material dumped over the edge of the pit. The 836 stope and the top of the 837 pillar had also been blasted resulting in additional sloughing of the hanging wall shear zone. The 834 stope was also enlarged. The resultant displacement of the pit wall is shown in Fig. 3.21(b). In three small areas displacement had increased to between 4 and 6 cm - around targets 2.5 and 5.1 and directly above the 836 stope. Most of the rest of the pit wall had a displacement of between 2 and 4 cm with a small area to the northeast still at less than 2 cm.

By the end of 1977 the middle portion of the 837 pillar had been blasted and the remaining part of the hanging wall shear zone sloughed. The 834 stope was slightly enlarged and the initial breakthrough of 830 stope had been made. The displacement of the pit wall is shown in Fig. 3.21(c). The pit wall above 834, 836, 837 and 838 stopes had now moved 4 to 6 cm with a small area above the larger opening having a displacement of between 6 and 8 cm. The rest of the pit wall with minor exceptions had moved 2 to 4 cm.

During 1978 there was no further blasting done in this area but the displacement continued to increase as shown in Fig. 3.21(d). Above the stope breakthroughs the maximum displacement was 8 - 10 cm with an increase in displacement in the central area of the southeast pit wall.

Figure 3.22 shows the total displacement of each target on a horizontal plane. The general movement had been directly into the pit. Those targets directly above the 836, 837 and 838 stopes showed a distinct change in vector direction towards this opening when these stopes were blasted and especially when the 836 stope was blasted.

Figure 3.23 illustrates the total displacement of each target on seven vertical sections through the pit wall. Below the ramp in sections 4, 5, 6 and 7, which is the area above the stope breakthroughs, the displacements were fairly consistent in a downward direction of about 30°. Above the ramp and for sections 1, 2 and 3 the displacements were more horizontal and in a few instances upward displacement had been measured.

Enough measurements have been made over a sufficient time span to examine the time-displacement aspects as shown in Fig. 3.24 for target on section 6. Up to the end of 1976, there was a distinct cause-and-effect relationship between mining activity and displacement. Movement occurred when the 838 crown pillar was blasted, but from mid-1975 to mid-1976 when no mining took place there was also no significant additional displacement. Movement was reactivated by the 836 and 837 crown pillar blasts at the end of 1976. After this the displacements were more time-dependent and the rate of displacement was greatest for the target at the bottom of the slope (6.5) and progressively decreased towards the pit crest. This behaviour could indicate a weathering type action causing the pit wall to move progressively into the pit. Alternatively, the middle portion of the 837 pillar was blasted during this period and the muck pile in the stopes had been drawn down, which would reduce the constraint

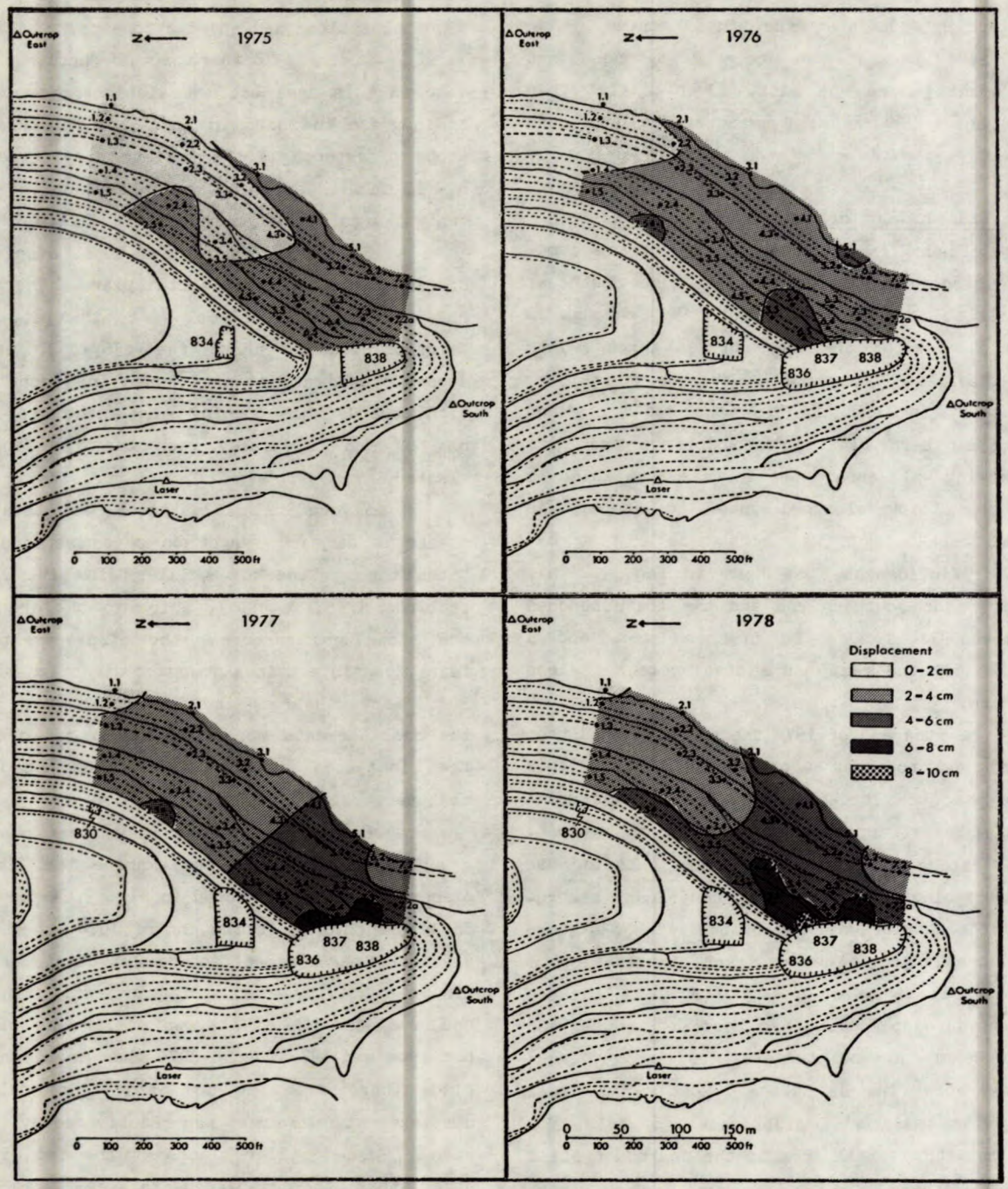

Fig. 3.21 - Total displacement distribution at the end of years 1975 to 1978

applied to the hanging wall. Which mechanism is prevalent, will only be determined by further measurements.

A comparison of the measured displacements and those predicted from 2-D and 3-D FE models is given in Fig. 3.25. Targets on sections 4 and 6 most closely resemble the sections modelled and the measured displacements are those at the end of 1976, when the distinct cause-and-effect response of displacement with mining ended. As can be seen, the measured displacements fell between those predicted from the two models. The

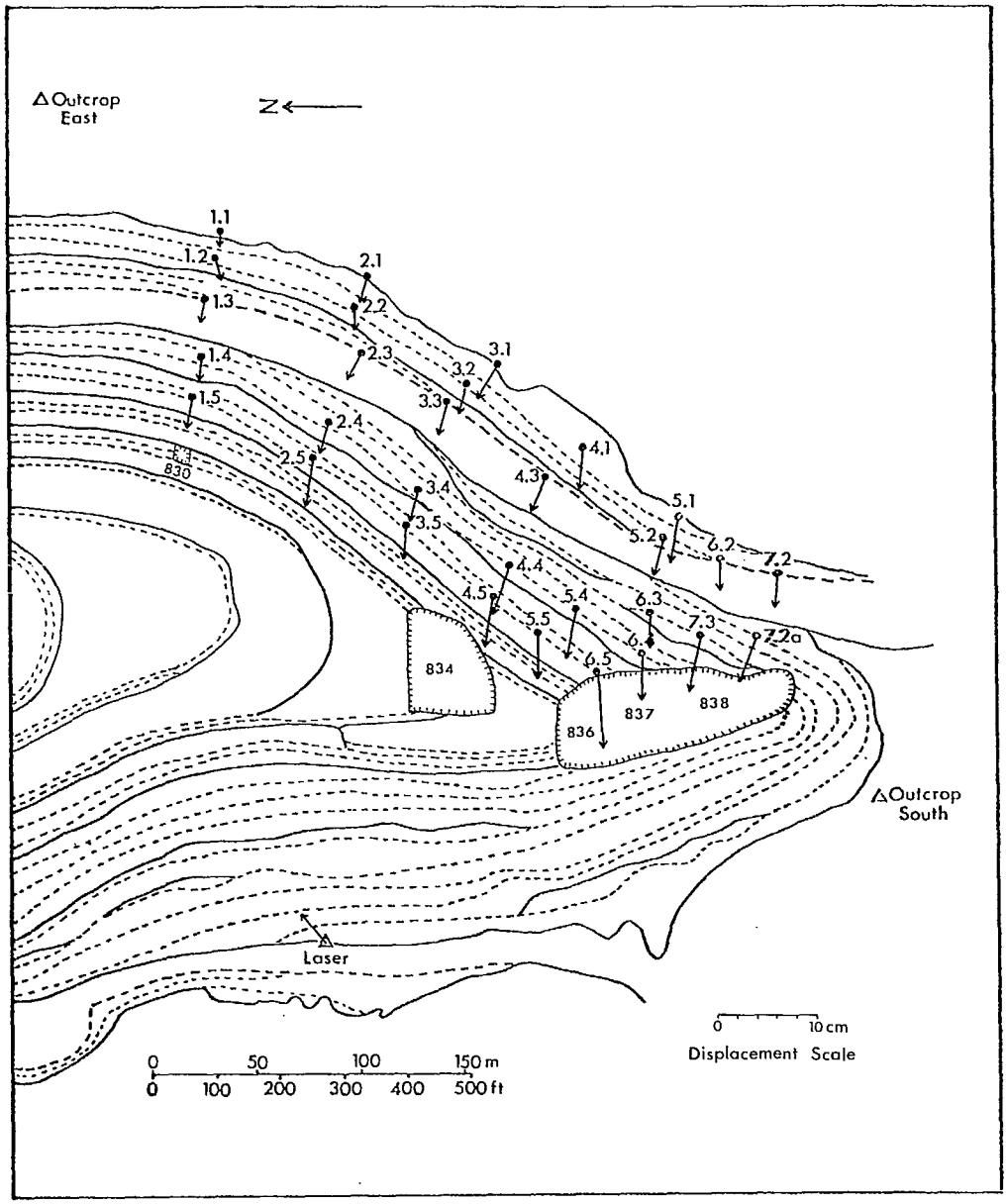

Fig. 3.22 - Displacement vectors in a horizontal plane at the end of 1978

2-D model predicted larger displacements and the 3-D model less. Direction is more similar to the 2-D model. These results are to be expected as the actual geometry is greater than that modelled in three dimensions, but less than that modelled in two dimensions.

3.7.3. Discussion on Displacement Measurements

A number of salient features brought out by the five years of measuring the southeast pit wall are worth noting. The measured displacements were consistent with each other. In other words, there were no large discrepancies between adjacent targets. This implies that the southeast pit wall was acting as a unit rather than as individual pieces of loose rock.

It was observed that displacement generally occurred as a result of two phenomena:

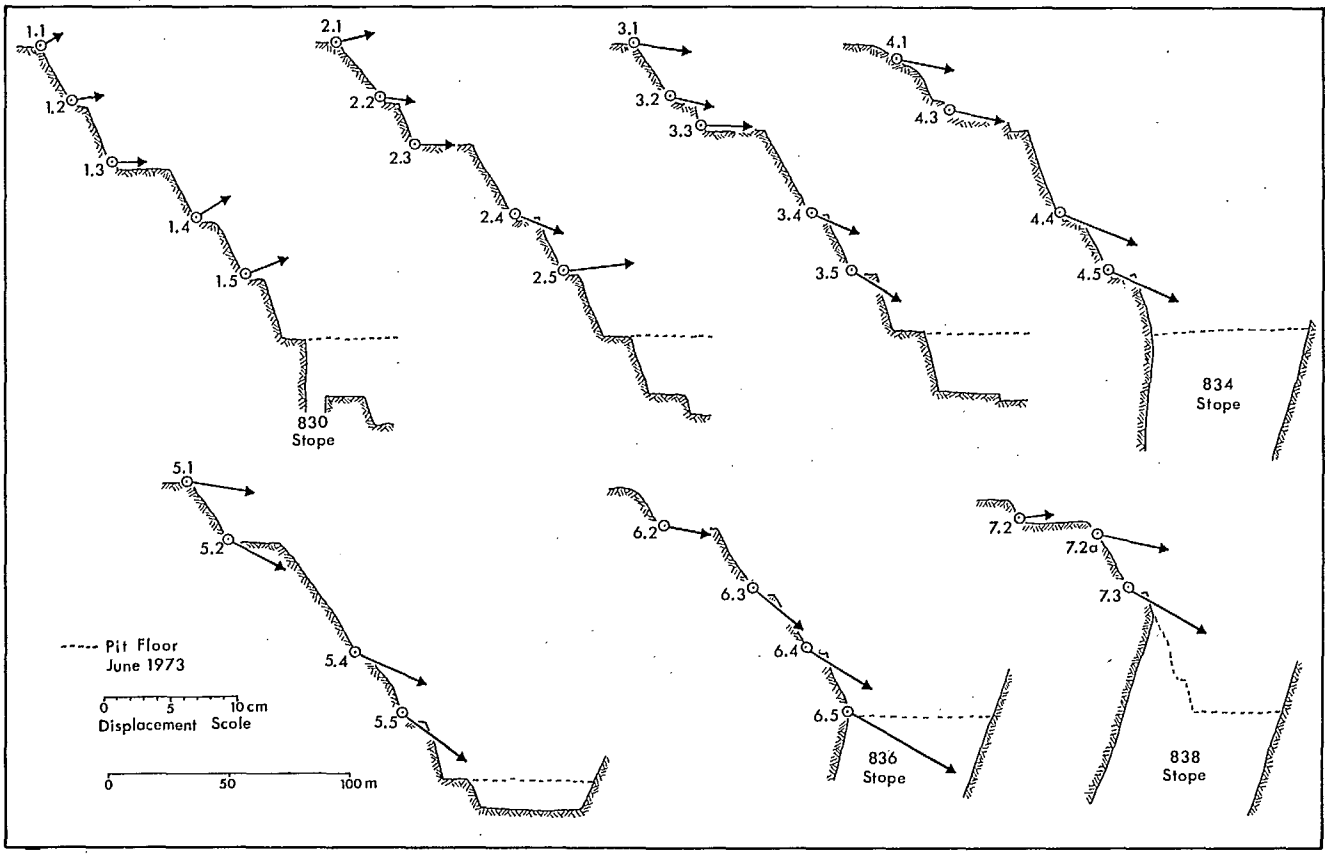

Fig. 3.23 - Displacement vectors in seven vertical sections at the end of 1978

a) blasting the stopes through into the pit resulted in a redistribution of stress and an inward movement of the hanging wall;
b) a weathering action probably due to rain, frost and ice which appeared to be prevalent after mining ceased in the area.

The maximum displacement measured so far is 9.2 cm on target 6.5 and the average displacement 4.3 cm. This overall displacement has not resulted in any visual deterioration of the pit wall. Benches are relatively free of loose rock and there are no visible tensile cracks either along the ramp or the pit crest. The only significant sloughing that has occurred is in the hanging wall shear zone at the southern end of the pit.

3.8. CONCLUSIONS

The initial objective was to monitor and evaluate stability of the southeast pit wall as it was undercut by mining. Geotechnical investigations on critical joint orientations and shear resistance along these discontinuities indicated that a plane or rotational shear type of instability was unlikely. This was confirmed by the 2-D FE model which predicts the redistribution of stress and resultant displacement due to mining. A yielding type of instability was investigated using a 3-D FE model. Again the results indicated that the hanging wall slope should be stable, although the hanging wall shear zone was predicted to slough, which in fact it did. Finally, measurements of slope displacement confirmed these

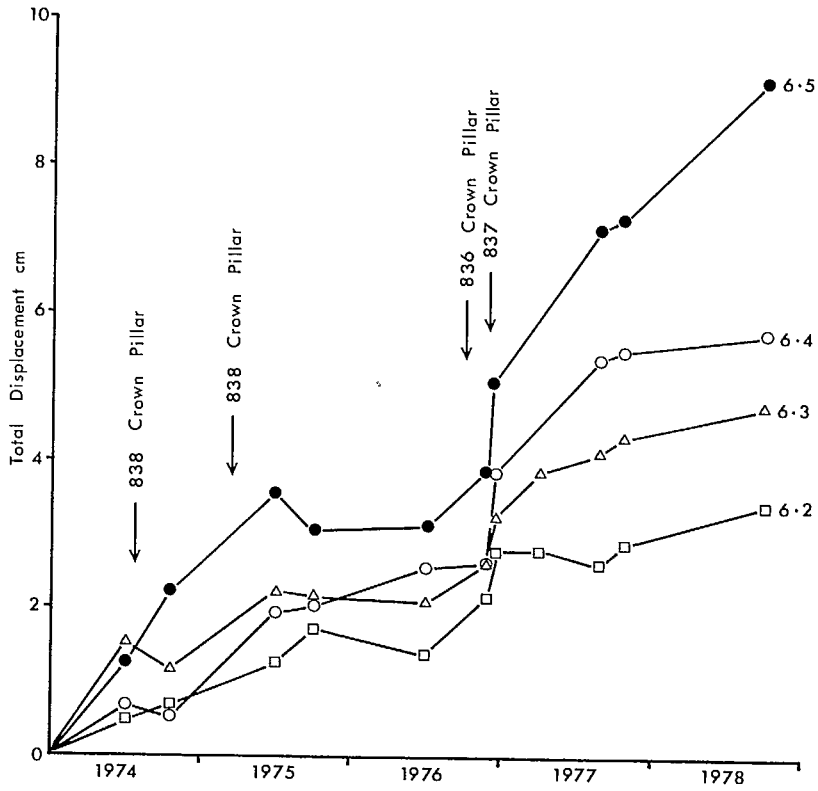

Fig. 3.24 - Total displacement with time for targets on section 6

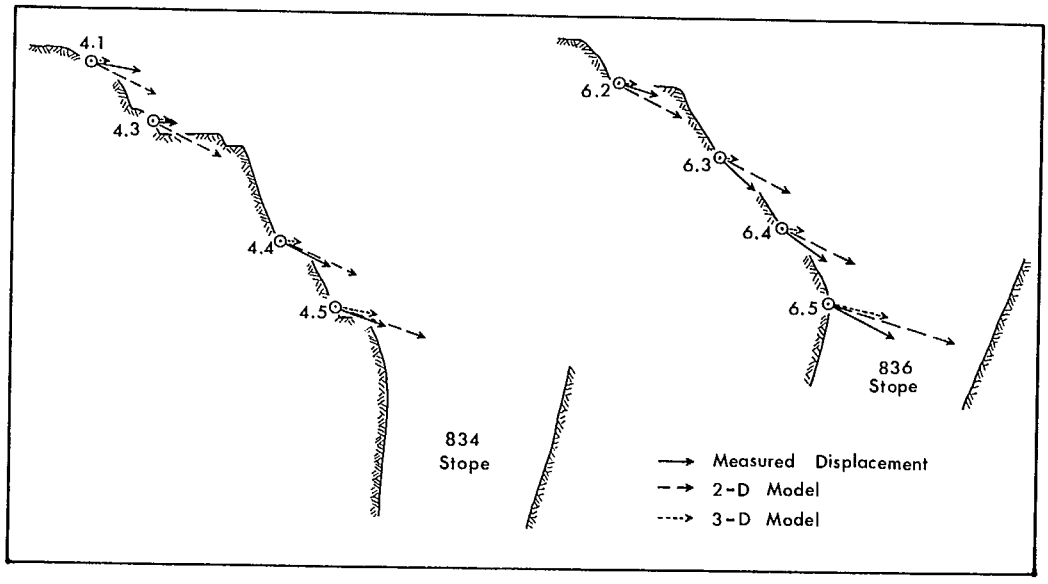

Fig. 3.25 - Comparison of measured and predicted displacement from 2-D and 3-D finite element models

studies. Displacement was consistent rather than erratic and showed a cause-and-effect relationship while mining was taking place. Magnitude of displacement fell within the limits predicted from the two FE models.

During the time these studies were being done, both the underground and open pit mines were in operation. Stopes were being blasted through at the southern end while the pit was being deepened at the northern end. Stability of the pit walls did not interrupt either operation and the pit was successfully completed in 1977.

This evaluation only covers the geometrical configurations analyzed. Further stopes are due to be blasted into the pit to the north of the area investigated and mining is progressing deeper. This will result in further redistribution of stresses and possible instability of the pit wall. It is intended to continue monitoring slope displacement as long as possible to detect any change in stability.

4. UNDERGROUND INVESTIGATIONS

A blasthole open stoping method with delayed cemented rockfill is used underground. The rock mechanics aspects of this mining system are concerned with the dimensions of the stope and pillars, sequence of extraction, and the effect these parameters have on stability of the pillars and stope walls. As basic input into any analysis is a knowledge of the pre-mining field stresses and their redistribution due to mining, deformational and strength characteristics of the orebody and surroundings. Measurements of field stesses, rock deformation around a stope and a preliminary evaluation of pillar stability are described in the following sections.

4.1. PRE-MINING FIELD STRESSES

Stress determinations were carried out with the CSIR doorstopper on 1600 (488 m), 2400 (731 m) and 2800 (853 m) levels and with the CSIR triaxial strain cell on 2800 level. Test sites were selected on the basis of uniform fine-grained rock types remote from active mining and operational interference. Locations in the footwall andesite/diorite were found to be the most suitable.

For the measurements on 2800 level a new strain cell installation tool was built in the Elliot Lake Laboratory which does not require compressed air for extrusion of rosette buttons. This tool performed well and overcoring was carried out with a PQ bit with an O.D. of 12.3 cm and an approximate core diameter of 8.5 cm. In competent rock the success rate was 71%. The two failures occurred while reading the strain cell during overcoring when drilling water shorted the electric circuit.

Drilling and overcoring of the doorstopper followed the well known procedure. Measurements were made from 4.6-m wide drifts 1.5 diameters from the drift boundaries.

Overcored specimens were subjected to quality testing of the strain gauge-rock bond and determination of physical properties. Results of the stress determinations are given in Tables 4.1 and 4.2. Directions of the maximum and intermediate principal stresses are given in Fig. 4.1. There is close agreement among the principal stress directions obtained on various levels and with different methods. The maximum principal compressive stress direction is about ENE - WSW / horizontal and for the intermediate stress about NNW - SSE / horizontal in relation to grid north.

Magnitudes are more variable and from earlier investigations stresses in vertical directions should approach overburden pressure (13). The stress determination sites in the footwall are predominantly overlain by andesite/diorite and a representative density for the overburden is 2900 kg/m^3. Calculated vertical pressures are shown in Table 4.1. Vertical stress component determined with the doorstopper method on the 1600 and 2800 levels and the triaxial results from 7.6 m on the 2800 level are in close agreement with the overburden pressure. High vertical and horizontal stresses on the 2400 level may be due to a large sheared zone of altered quartz porphyry approximately 30 m west of the test site.

Previous stress measurements in Northern Ontario (13) indicate that the average horizontal

Table 4.1 - Absolute ground stress tensor components in relation to grid north

Site/Method	Elastic modulus MPa	Poisson's ratio	Stress components MPa σ east	σ north	σ vert	τ EN	τ NV	τ EV	Calculated overburden stress, MPa
1600 level doorstopper	95.8	0.27	31.9	25.4	13.4	2.8	5.0	-3.7	13.8
2400 level doorstopper	80.0	0.27	62.9	65.1	43.9	6.4	-4.4	14.6	20.7
2800 level doorstopper	95.8	0.27	51.0	52.5	20.9	0.8	-0.1	7.5	24.2
2800 level triaxial 6.1 m	95.8	0.30	61.6	50.1	34.6	5.1	7.7	14.8	24.2
7.6 m	77.9	0.27	44.8	42.9	23.6	7.1	-1.1	14.7	24.2

Average standard error: doorstoppers 10%, triaxial 4%.
Grid north 20° clockwise from geographic north.

Table 4.2 - Principal stresses at Kidd Creek mine given in relation to Grid North in MPa

Site/Method	σ_1 Magnitude	σ_1 Direction /dip	σ_2 Magnitude	σ_2 Direction /dip	σ_3 Magnitude	σ_3 Direction /dip
1600 level - doorstopper	33.2	074/06	26.8	166/23	10.8	330/66
2400 level - doorstopper	72.6	239/19	64.7	338/25	34.4	115/58
2800 level - doorstopper	53.4	230/10	51.9	322/9	19.1	92/77
triaxial cell (6.1 m)	67.9	066/16	48.6	335/10	28.1	216/72
triaxial cell (7.6 m)	53.2	057/12	39.9	150/18	16.3	298/70

stress, σh, can be expressed by:

$$\sigma h = 8.00 + 0.041\ H \text{ in MPa}$$

where H is the depth in metres.

Figure 4.2 shows this relationship with the results from the Kidd Creek mine superimposed.

The measurements on the 1600 level and the triaxial results at 7.6 m on the 2800 level fall almost exactly on the predicted line. Other measurements are somewhat higher especially as noted on the 2400 level.

It is interesting to observe that the difference in stress magnitude between the two horizontal stresses (Table 4.1) of 7 to 14 MPa is fairly marginal and decreases with increasing depth. This would suggest that orienting mine openings in the more favourable direction of maximum principal stress probably would not have a significant effect.

4.2. UNDERGROUND DEFORMATION MEASUREMENTS

Stope 838 at the extreme southern end of the orebody was the first production stope started early in 1973. Figure 4.3 shows an east-west vertical section through this stope. The orebody varies in width from 9 m at the 800 level to about 45 m at the crown pillar. The immediate contact

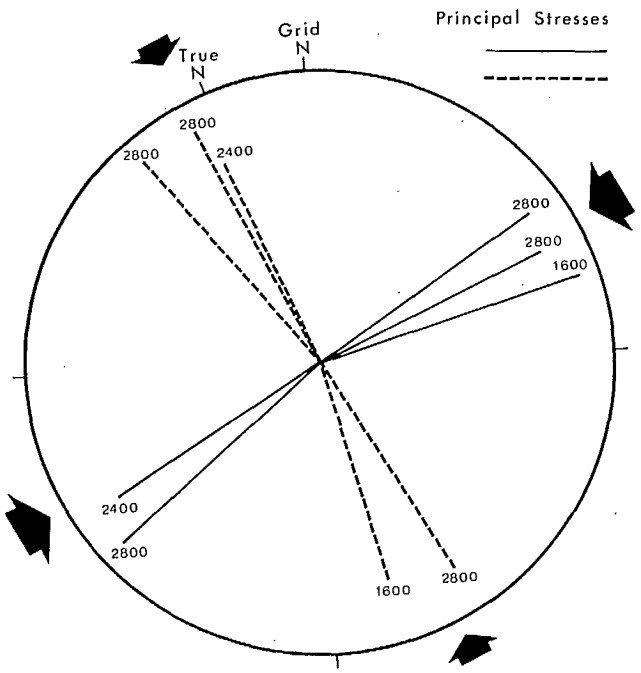

Fig. 4.1 - Plot of major (σ_1) and intermediate (σ_2) principal stress directions for 1600, 2400 and 2800 levels in lower hemisphere of equal area net

on the hanging wall is the Ancillary shear zone and on the footwall the North-South shear zone. Both these zones are characterized by intensive shearing and breakdown of the rock material and could spall into the open stope. The stope extends from the 800 level to just above the 8-3 sub-level, a height of 98 m. The crown pillar between the stope and open pit varies in thickness from 50 m to 90 m at the southern end.

Borehole extensometers were installed around the 838 stope prior to any major mining activity. A multi-wire type installation was used. Basically this involves anchoring several stainless steel wires at different depths in a borehole. A constant tension is applied to each wire and the extensometer measures the position of the end of the wire, and hence the anchor, relative to the collar station to within 0.025 mm.

4.2.1. Layout of Borehole Extensometers

Six borehole extensometers were installed on the 8-2 and 8-3 sub-levels. Figure 4.4 shows a plan of the 8-2 sub-level and the blasting sequence on this sub-level. Boreholes M1 and M2 were drilled slightly downwards and perpendicular to the strike from the footwall access drift through the footwall shear zone. M1 was located opposite the middle of the 837 stope and M2 opposite 838 stope. Four wires were installed in each borehole.

Boreholes M3 and M4 were drilled from the central crosscut through the 838 pillar, approximately at the mid-point of the pillar. M4 was drilled horizontally 4.6 m towards the 838 stope and three wires were installed. Borehole M3 was 12.2 m long and inclined upwards at 20° so that it passed over the top of the 837 slot drift and six wires were installed in this borehole. On the 8-3 sub-level, boreholes M6 and M7 were identical to M3 and M4.

4.2.2. Sequence of Extraction

Figure 4.5 is a north-south longitudinal section showing the blasting sequence for the block of stopes and pillars at the southern end of the orebody. The locations of the borehole extensometers are also shown on this section. At the beginning of measurements in January 1973, the planned sequence of extraction was to mine 838 stope first, followed by 837 and 836 stopes. De-

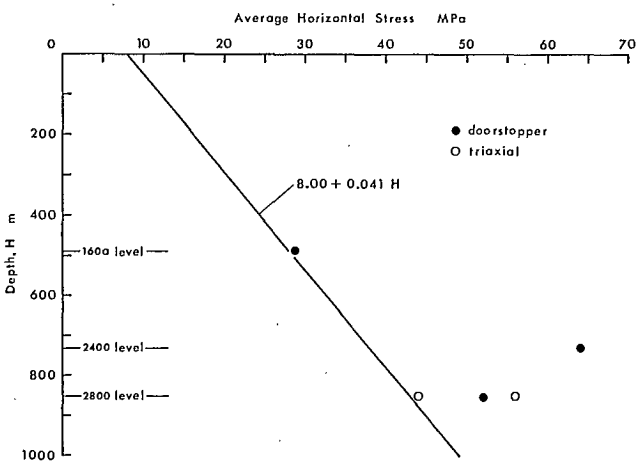

Fig. 4.2 - Variation in average horizontal stress with depth.

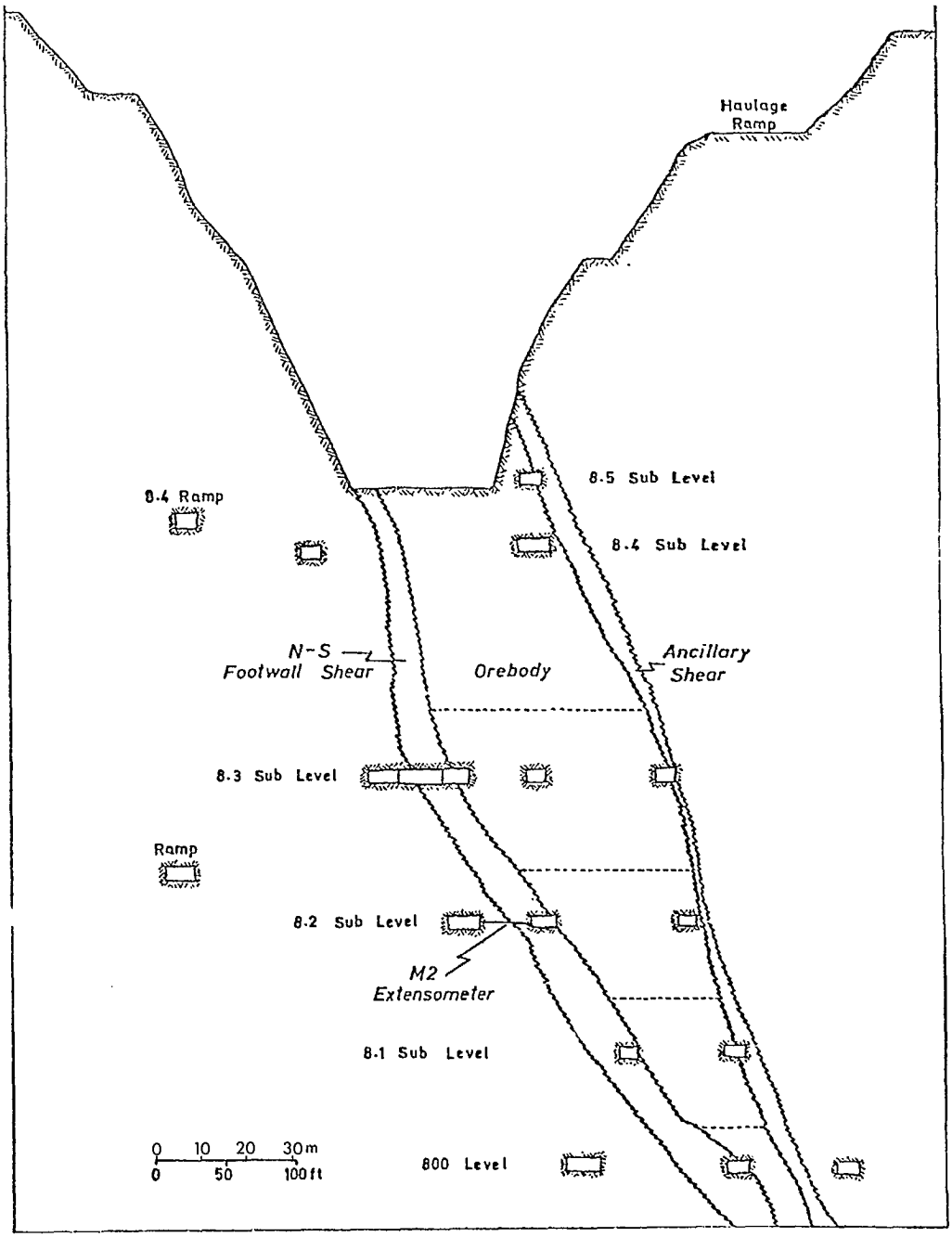

Fig. 4.3 - East-west vertical section through 838 stope.

pending on ground conditions, these stopes could be filled with cemented rockfill prior to mining the 15-m wide rib pillars. This sequence of extraction was subsequently changed and 838 pillar and part of 837 stope were mined immediately after 838 stope. This enlarged stope was then filled with cemented rockfill as shown in Fig. 4.5. The 836 stope was mined through into the open pit followed by blasting of the 837 pillar and the remaining part of the 837 stope from the top downwards. A 27-m wide permanent pillar to the north of 836 stope separated the next block of stopes and pillars.

The general method of extraction within a stope is first to excavate the undercut slot above the drawpoints by a 3-m wide slot next to

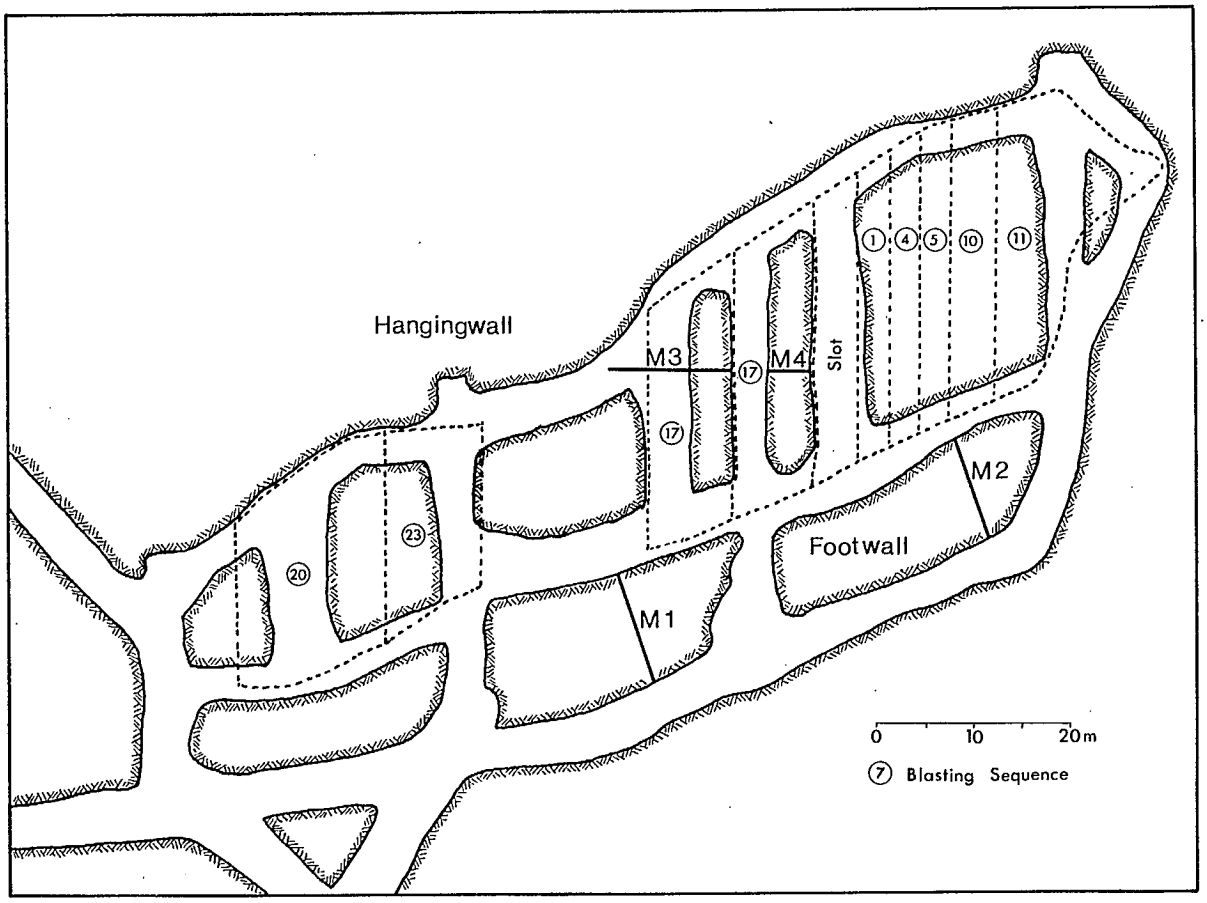

Fig. 4.4 - Plan of 8.2 sub-level showing layout of borehole extensometers

the pillar or at the centre of the stope. Rings spaced at 1.5-m intervals are progressively blasted into the slot. Blasting in the lower sublevels is kept ahead of the ones above to form a rilled face configuration. On completion of blasting in a stope, the slot is extended into the open pit and the crown pillar is removed in one or two large blasts.

4.2.3. Footwall Shear Zone Deformation

Figure 4.6 shows the deformation measured on boreholes M1 and M2 between 1973 and 1977. Movement of each wire and hence of the anchor relative to the borehole collar is plotted and the vertical distance between curves represents the deformation which has occurred between anchors. The number and time of each blast are also shown which allows a cause-and-effect relationship to be established (Fig. 4.5).

Considerable deformation was measured in the M2 borehole opposite the 838 stope and it should be noted that the deformation scale is in centimetres compared with millimetres on the other graph. The first deformation occurred after blasts 4 and 5 when the edge of the stope was opposite the borehole (Fig. 4.4 and 4.5). Deformation was mainly confined to an expansion of 0.2 cm on the 1.5-m wire. A compression of 2.2 cm was recorded on the 4.6-m wire, but this is thought to be slippage of the anchor or wire. Consequently, this reading was corrected and subsequent movement of this wire mirrored movements on the other wires.

Blasts 6, 7 and 9 on the 8-3 sub-level

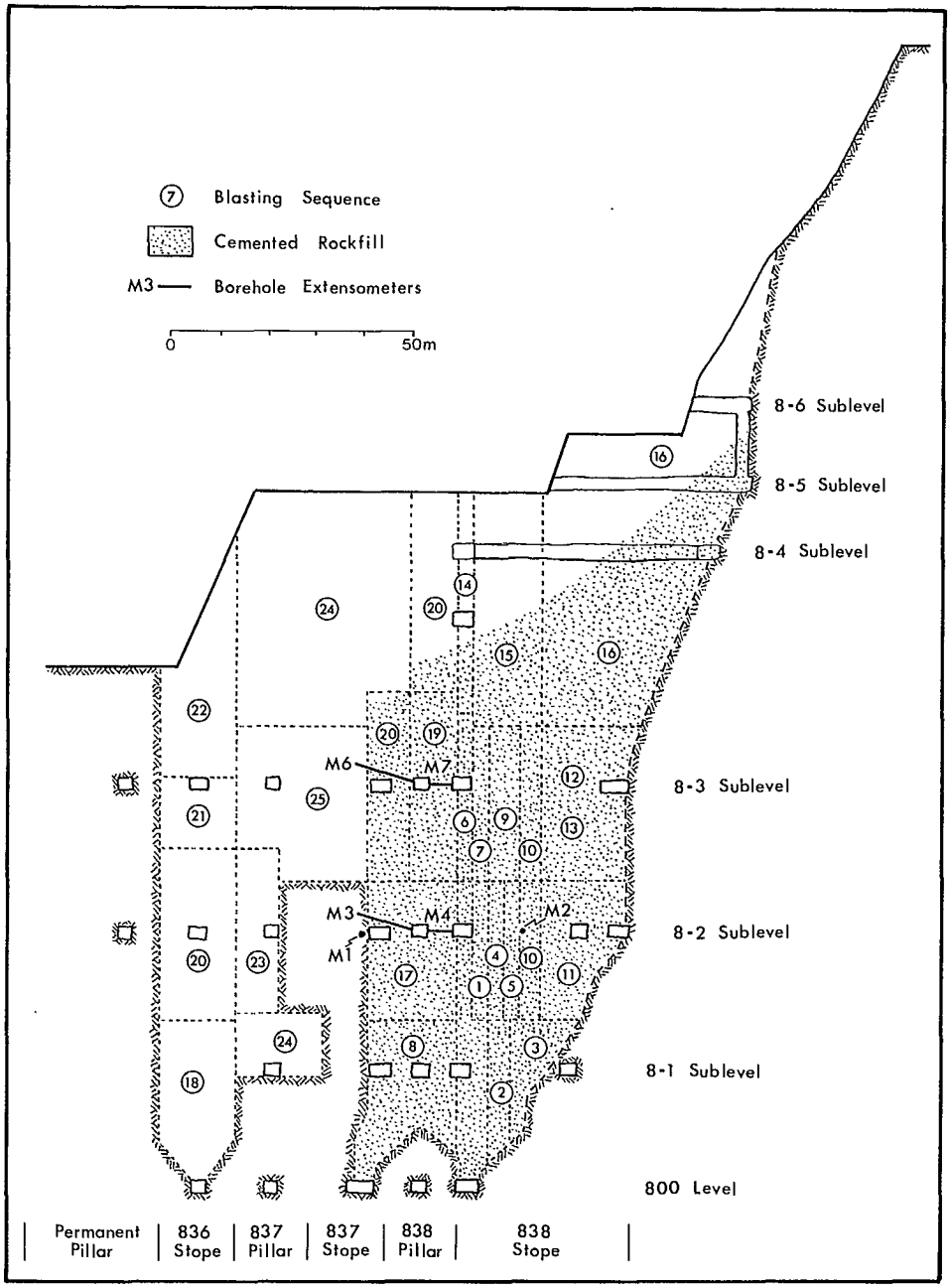

Fig. 4.5 - Longitudinal section showing sequence of extraction at southern end of orebody.

had no noticeable effects on the borehole. Deformation was reactivated, mainly on the 7.6-m and 10.7-m wires, by blasts 10 and 11 on the 8-2 sub-level and to a lesser extent blast 12 on the 8-3 sub-level. At this point, with expansion of the shear zone in the range of 1.8 cm, a cable bolting program was initiated opposite 838 stope from the footwall access drift on the 8-2 sub-level. Boreholes were drilled at 15° and 30° downwards, alternating at 1.5-m intervals along the drift. Old hoisting cables 3.2 cm in diameter were grouted in these boreholes which stopped just short of the open stope. A similar cable bolting installation was also done on the 8.3 sub-level.

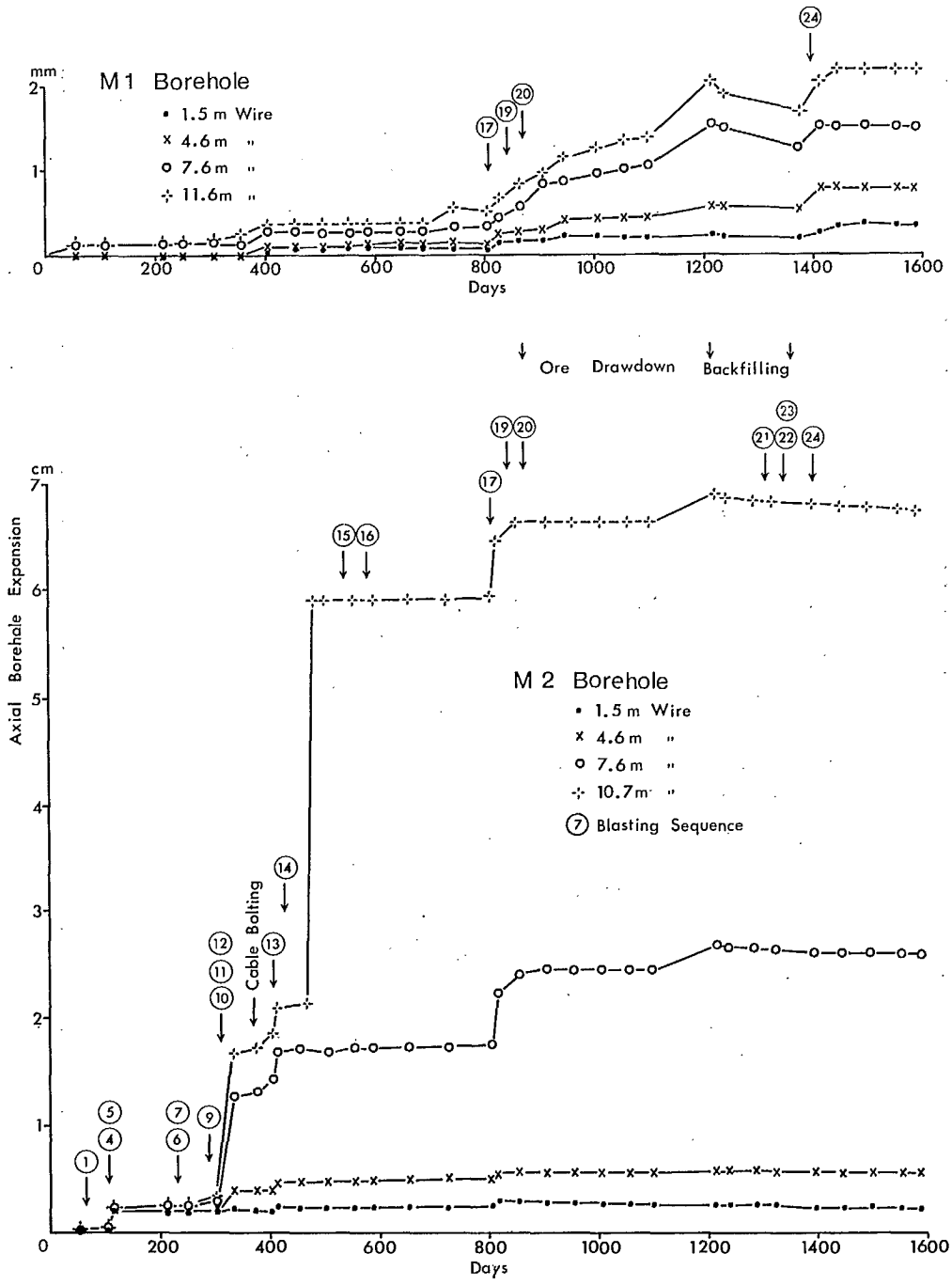

Fig. 4.6 - Deformation of footwall rocks measured in boreholes M1 and M2

Expansion of the shear zone continued during installation of these cable bolts with additional movement due to blast 13 on the 8-3 sub-level.

Blasts 14, 15 and 16 in the crown pillar had no noticeable effect on the borehole. However, between blasts 14 and 15, the 10.7-m wire showed a sudden expansion of 3.8 cm which would indicate a breakdown of the outside few metres of the shear zone. This may have been due to lowering the broken ore below the 8-2 sub-level and removing the constraint of this broken material.

Deformation was reactivated on the 7.6-m wire by pillar blast 17 on the 8-2 sub-level and to a lesser extent by blasts 19 and 20 on the 8-3

sub-level. Blast 17 also activated deformation on borehole M1 which up to this time had shown little deformation, the edge of the stope being opposite this borehole.

Following blast 20 there was no active mining in the area for a period of 500 days. During this time the two longest wires in each borehole indicated a gradual expansion followed by compression, which is most noticeable on the M1 borehole as the scale is magnified.

Expansion of the footwall shear zone coincided with drawdown of the broken ore in 838 stope and there was an acceleration in the late stages, presumably as the muck level approached the horizon of the extensometers. On commencement of backfilling in 838 stope, the movement reversed and went into compression and recovered about one third of the expansion which occurred during ore drawdown. This behaviour would indicate that the broken ore in a stope has an effect on movement of the walls. Prior to the final ore drawdown, movement of the footwall shear zone was mainly related to blasting with the resultant redistribution of stresses and an increase in stope span. During drawdown the shear zone exhibits a type of time-dependent deformation. This evidence would suggest that the stopes should, as much as possible, be kept full of broken ore during stoping operations, which is almost equivalent to shrinkage stoping, and that the time interval between commencing final drawdown and backfilling should be kept as short as possible.

Prior to the final ore drawdown and backfilling, the measurements in M2 borehole showed a clear cause-and-effect relationship between blasting and displacement. Essentially, blasts on the same sub-level have the major effect. In other words, the lateral stope span is the predominant parameter which controls inward displacement of the footwall shear zone. The shear zone contact is located between the 4.6 m and 7.6 m anchors and the displacement measured on the 7.6 m wire would represent the movement of this contact.

Figure 4.7 shows the relationship between stope span and displacement of the shear zone contact. Although there are only three points plus the origin, there is reasonable agreement with a straight line. Displacement after blast 5 with a stope span of 13 m is low, but the stope face was only opposite the borehole at this time. The results indicate that the shear zone is not acting like a beam where the expected relationship would be that displacement is proportional to stope span to the fourth power. Normal stope spans are about 18 m and from the graph the expected displacement of the shear zone for these stopes would be about 8 mm.

4.2.4. Pillar Deformation

Deformations measured in boreholes M3 and M4 on the 8-2 sub-level are shown in Fig. 4.8. Again, Fig. 4.4 and 4.5 should be referred to for the blasting sequence. The six wires in borehole M3 indicated a gradual lateral expansion due to blasts 1 to 13 with the crown pillar blasts 14, 15 and 16 having very little effect. Total measured movement on the longest wire amounted to about 2 mm.

In the M4 borehole, lateral expansion is limited to the 3.0-m and 4.3-m wire which is at the edge of the pillar. Blasts 10, 11, 12 and 13 had the major effect and again blasting of the crown pillar had no noticeable effect. Expansion was reactivated on the two wires at the beginning of 1975 when there was no mining activity in the area. This is thought to be caused by lowering the broken ore in the stope and removing constraint on the pillar side. Blast 17 removed both of these borehole extensometers.

Boreholes M6 and M7 on the 8-3 sub-level were duplicates of M3 and M4 on the 8-2 sub-level. Also the distribution and magnitude of the deformations were very similar up to blast 17 . This blast undercut the pillar 18 m below the 8-3 sub-level and produced 4 mm expansion on both 1.5-m wires on either side of the pillar crosscut. Shortly after the blast, and prior to taking any readings, the edge of the pillar caved, taking out the 3.0 m and 4.6 m wires in the M7 borehole. Prior to blast 17, total deformation amounted to only 0.8 mm with no indication of any fractures developing.

This information indicates that under-

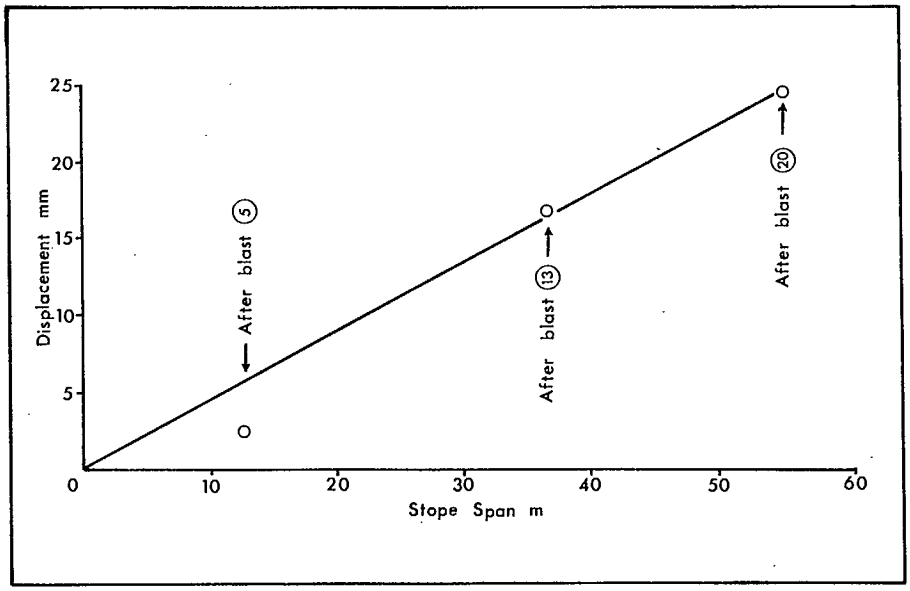

Fig. 4.7 - Effect of stope span on displacement of footwall shear zone

cutting of both pillars and stopes could result in caving of the brows with little or no warning. In the absence of other criteria, blasting of vertical slices, rather than a rill face, in a retreating sequence would provide a more stable configuration.

In general, lateral pillar deformation is an order of magnitude less than deformation of the footwall shear zone, i.e., in mm compared with cm. On a cause-and-effect basis it is mainly the blasts adjacent to the boreholes which produce the lateral expansion. Again, there is an indication that the broken ore in the stope produces a significant constraint on the pillar side, which when removed, results in additional expansion into the stope.

4.3. EVALUATION OF PILLAR STABILITY

Instability of a pillar can result from two processes. The geological structure and the friable nature of the rock may be such that when constraint is removed by mining in the stopes the walls slough or the back caves under its own weight. Alternatively, the stresses transferred to the pillar during stoping may exceed the rock mass strength of the pillar causing sloughing and in the extreme cases complete pillar disintegration. In the former case, pillar stability with increasing depth will depend on the geological conditions encountered, whereas in the latter case, occurrences of pillar instability will increase with increasing depth as the stresses will be greater for a constant layout of stopes and pillars.

A preliminary study was done to estimate the strength of pillars and stresses applied to them, to see if this failure mechanism could explain the number of cases of pillar sloughing that have occurred.

4.3.1. Estimation of Pillar Stresses

In situ measurements have indicated that the horizontal field stresses can be expressed as:

$$\sigma h = 8.00 + 0.041\ H$$

where H = depth in metres.

East-west horizontal stress is the major stress acting through the transverse rib pillars. There are three stages in the stress transfer sequence due to mining:

a. Excavating the open pit transferred the hori-

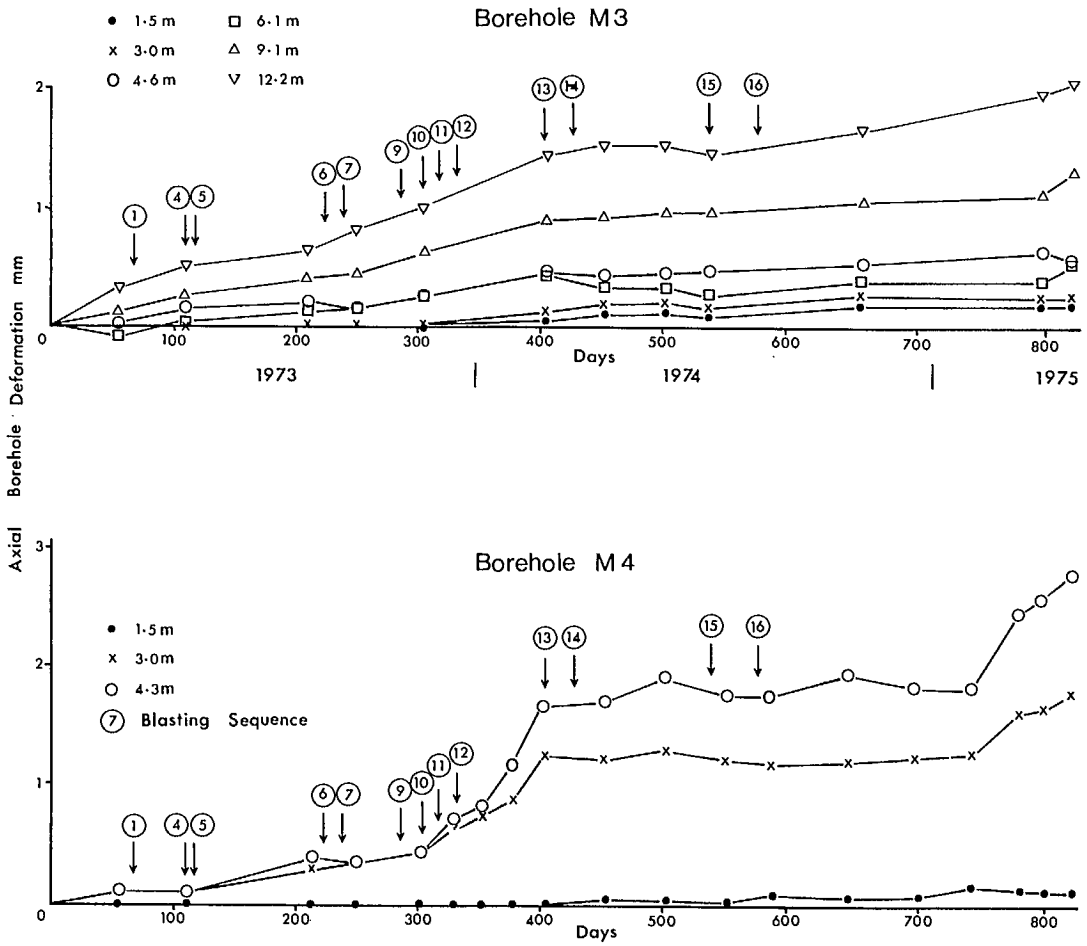

Fig. 4.8 - Lateral pillar deformation measured in boreholes M3 and M4

zontal stress beneath the pit floor. The 3-DFE model estimated a concentration factor of about 2.0 on the pit floor, which reduced with depth and reached field stress conditions at about 250 m depth.

b. Mining the stopes results in a further redistribution of stress to the rib and crown pillars.

c. Finally, pillar recovery operating cause stress to be diverted to the remaining rib and crown pillars, and to a lesser extent the cemented rock backfill will support some load depending on how much it is compressed.

Estimating pillar stress is difficult under these conditions and under varying geometry. As a first approximation the stopes and pillars on the 1200 level were analyzed as in most cases they were far enough below the pit floor not to be significantly affected by stress transfer due to excavating the pit. Also no pillar recovery operations had started and a few pillar walls had sloughed while mining the stopes.

On the 1200 level there are 13 stopes and 12 intervening rib pillars spaced out over a distance of 550 m along strike. Stopes are 18 m wide by 80 m high and the length varies from 12 m to 60 m in the hanging wall to footwall direction. Rib pillars are 24 m wide with crown pillars 18 m and 24 m thick above and below. Depth below surface to the centre of the pillars is about 300 m.

When mining operations are extensive the average stress acting on the central pillars can be approximated by the tributary area theory. This states that a pillar supports the pre-mining stress on itself plus half of each adjacent stope, which can be expressed as:

$$\sigma p = \frac{\sigma h}{1 - R}$$

where: σp = average pillar stress, MPa

σh = horizontal field stress, MPa

R = extraction ratio

The upper and lower limits of the extraction ratio can be taken respectively as the 2-D case at mid-pillar height and the 3-D case which includes the crown pillars. For the stope and pillar dimensions listed above.

R(3-D) = 0.43 and R(2-D) = 0.34

At a depth of 300 m average pillar stress for the two extraction ratios are:

σp = 36 MPa for R = 0.43

σp = 30 MPa for R = 0.33

Higher stresses would be expected at the pillar edges and especially at the corners. Finite element models of pillars similar to those at the Kidd Creek mine indicate a stress concentration factor of about 1.3 at the pillar edge and 1.55 at the corners compared with the average pillar stress. Consequently, the range of pillar stresses on the 1200 level are likely to be:

	Pillar Stress, MPa		
	Average	Pillar edge	Pillar corner
Extraction 0.43	36	46	55
Extraction 0.33	30	39	47

4.3.2. Estimation of Pillar Strength

It is known that the rock mass strength of mine pillars is much less than the strength of small intact samples tested in the laboratory. Besides this shape and size effect, pillar strength is also affected by factors such as its width to height ratio and ratio of exposed surface area to cross-sectional area.

Most empirical equations relating pillar strength to its width and height were derived in Imperial units (14, 15). The general equation is:

$$Qu = K \frac{W^a}{H^b}$$

where: Qu = pillar strength, psi

W = pillar width, ft

H = pillar height, ft

K = strength of a foot cube

a and b = constants.

Values of the constants quoted in the literature are: a = 0.50 and b = 0.50 to 1.00. Most of the testing has been done on coal and the one hard-rock example used b = 0.75 (15). As the size of the rib pillars is far beyond previous evaluations of pillar strength, two values of b equal to 0.65 and 0.75. were analyzed.

This empirical equation is dimensionally correct only when the exponents a and b are equal, which is not the case, and this poses a problem in converting into metric units. To maintain consistency of units a coefficient α can be inserted as follows:

$$Qu = \alpha K \frac{W^a}{H^b}$$

In Imperial units α would have the dimensions 1 $ft^{(b-a)}$ which equals 1, whereas in metric units α would have the dimensions 0.305 $m^{(b-a)}$. For the two sets of exponents analyzed the values for α are:

α = 0.50, b = 0.75 a = $.305^{.25}$ = 0.743

α = 0.50, b = 0.65 a = $.305^{.15}$ = 0.837

The original pillar strength equation can now be expressed by:

b = 0.65 $\quad Qu = 0.837\ K \frac{W^{.5}}{H^{.65}}$

b = 0.75 $\quad Qu = 0.743\ K \frac{W^{.5}}{H^{.65}}$

where: K = strength of 0.305 metre cube, MPa

W and H = pillar width and height, m.

Uniaxial compressive strength tests were described in Section 3.1. Samples had a length to diameter ratio of 2:1 and four different diameters. There was an increase in strength from 32-mm to 41-mm diam samples, then a consistent decrease to 245-mm diam samples. The 41-mm diam samples were used as a reference size. An empirical strength to size relationship was determined for the three major rock types of andesite, rhyolite and ore according to the equation:

$$\frac{Q_B}{Q_O} = \left(\frac{D_B}{D_O}\right)^{-c}$$

where: Q_B = strength of sample diameter, D
Q_O = strength of reference specimen
D_B = sample diameter
D_O = diameter of reference specimen.

A total of 75 test results were available for regression analysis and the normalized values are shown in Fig. 4.9. Exponent c was found to be 0.16 and the strength of a 300-mm diam sample was estimated as being 72% of the 41-mm diam reference samples.

The effect of length to diameter ratio on laboratory strength has been determined as follows (16):

$$\frac{Qc}{Q_1} = 0.778 + \frac{0.222}{L/D}$$

where: Qc = strength of sample with L/D ratio other than 1
Q_1 = strength of sample with L/D = 1
L/D = length/diameter ratio, in this case 2:1

The mean strength of a 300-mm cube based on the reference sample of 41-mm diam can now be expressed as:

$$Q_1 = \frac{0.72\ Qc}{0.889}$$

This yields for the three major rock types:

	Strength of 30-cm cube
ore	129.5 MPa
andesite	163.9 MPa
rhyolite	119.4 MPa

Using the strength of the ore in the pillar strength equations gives:

b = 0.65

$$Qu = 0.837 \times 129.5 \frac{W^{.5}}{H^{.75}} = 108 \frac{W^{.5}}{H^{.75}}$$

b = 0.75

$$Qu = 0.743 \times 129.5 \frac{W^{.5}}{H^{.75}} = 96 \frac{W^{.5}}{H^{.75}}$$

At the Kidd Creek mine the orebody is almost vertical and the horizontal stresses are greater than the vertical stress. In this case the pillar is considered to be horizontal and its height is equivalent to its length, L, perpendicular to the strike, i.e., hanging wall to footwall. Hence L can be substituted for H in the pillar strength equations.

However, this analysis has been taken far beyond the range of existing knowledge or experience, especially for the strength of the large pillars. As such, the analysis outlines a

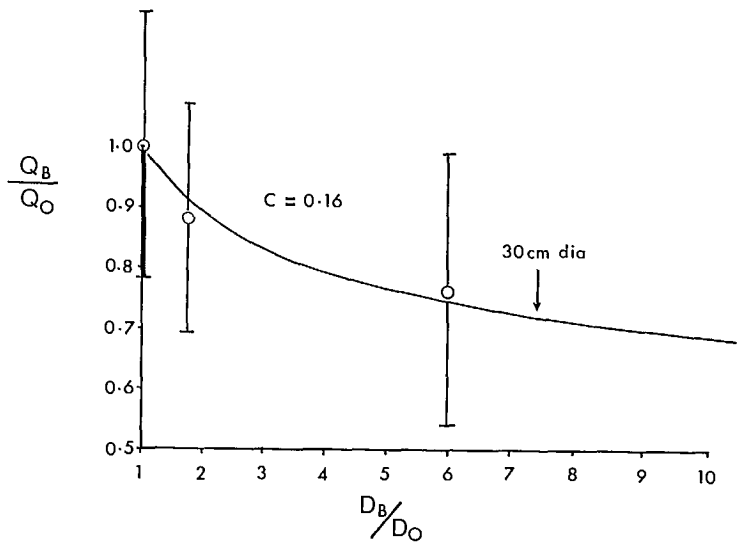

Fig. 4.9 - Relationship between specimen size and strength for Kidd Creek rock types.

$$\frac{Q_B}{Q_0} = \left(\frac{D_B}{D_0}\right)^{-c}$$

where: Q_B = strength of sample diameter, D
Q_0 = strength of reference specimen
D_B = sample diameter
D_0 = diameter of reference specimen.

A total of 75 test results were available for regression analysis and the normalized values are shown in Fig. 4.9. Exponent c was found to be 0.16 and the strength of a 300-mm diam sample was estimated as being 72% of the 41-mm diam reference samples.

The effect of length to diameter ratio on laboratory strength has been determined as follows (16):

$$\frac{Qc}{Q_1} = 0.778 + \frac{0.222}{L/D}$$

where: Qc = strength of sample with L/D ratio other than 1
Q_1 = strength of sample with L/D = 1
L/D = length/diameter ratio, in this case 2:1

The mean strength of a 300-mm cube based on the reference sample of 41-mm diam can now be expressed as:

$$Q_1 = \frac{0.72\ Qc}{0.889}$$

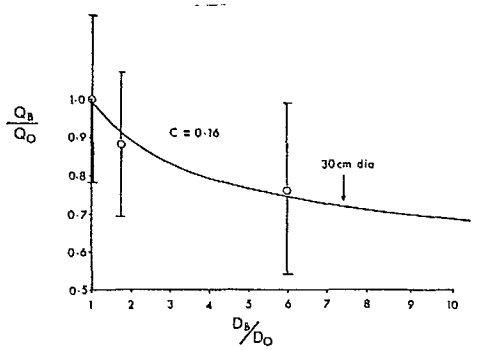

Fig. 4.9 - Relationship between specimen size and strength for Kidd Creek rock types.

This yields for the three major rock types:

	Strength of 30-cm cube
ore	129.5 MPa
andesite	163.9 MPa
rhyolite	119.4 MPa

Using the strength of the ore in the pillar strength equations gives:

b = 0.65

$$Qu = 0.837 \times 129.5 \frac{W^{.5}}{H^{.75}} = 108 \frac{W^{.5}}{H^{.75}}$$

b = 0.75

$$Qu = 0.743 \times 129.5 \frac{W^{.5}}{H^{.75}} = 96 \frac{W^{.5}}{H^{.75}}$$

At the Kidd Creek mine the orebody is almost vertical and the horizontal stresses are greater than the vertical stress. In this case the pillar is considered to be horizontal and its height is equivalent to its length, L, perpendicular to the strike, i.e., hanging wall to footwall. Hence L can be substituted for H in the pillar strength equations.

On the 1200 level, pillar width is standardized at 24 m. The few instances of pillar sloughing have occurred at pillar lengths ranging from 33 to 43 m. However, there are more cases where pillar sloughing has not occurred with lengths ranging from 12 to 61 m.

The estimated strengths for those pillars which have had some sloughing are:

Pillar length	Pillar strength, MPa	
	b = 0.65	b = 0.75
33 m	54	34
43 m	46	28

4.3.3. Pillar Stability

Estimates of pillar stresses for the 1200 level pillars indicate an average stress of 30 to 36 MPa, a concentration on the pillar edges of 39 to 46 MPa, and at the pillar corners of 47 to 55 MPa. As sloughing is confined to the edges of the pillars, failure is more likely due to the stress concentrations at the edges and corners. Estimated pillar strengths of 46 to 54 MPa from the equation:

$$Qu = 108 \frac{W^{.5}}{L^{.65}}$$

give closer agreement to the pillar stresses than when an exponent b = 0.75 is used.

However, this analysis has been taken far beyond the range of existing knowledge or experience, especially for the strength of the large pillars. As such, the analysis outlines a

possible engineering approach to pillar stability rather than providing design guidelines.

Measurements of pillar stresses at the time sloughing is occurring is required to validate predictions of both stress and strength.

Notwithstanding the preliminary nature of the pillar stability analysis a number of general conclusions can be made on improving pillar stability. Strength of a pillar increases with increasing width and decreases with increasing length. Of these two dimensions the length has probably the greater effect on strength. Where the orebody is wide - about 60 m between hanging wall and footwall - it may be possible to mine the stope in two stages. First would be a 30-m long stope against the hanging wall which would be bulk filled prior to mining the second stope 30 m long against the footwall. This would limit the exposure of the pillar side to 30 m rather than 60 m if the stope were mined as one unit.

A rib pillar is in its weakest condition when stopes on both sides are extracted and empty. In this case the exposed surface area of the pillar is at a maximum. After the stopes have been backfilled, the backfill itself is in its weakest condition when the pillars on both sides are extracted and empty.

Both these weakest conditions can be eliminated by sequencing the extraction as shown in Fig. 4.10.

The basic building block consists of 5 units and it takes 5 stages of mining and backfilling to complete extraction. In no stage is an ore or backfill pillar left unsupported on both sides. 40% of the units are mined with ore walls on either side, 20% with one ore wall and one fill wall and 40% between fill walls.

4.4. CONCLUSIONS

The initial objective was to contribute to the design of the underground mining method by examining ground control aspects.

Field stress measurements indicated that the stress regime at the Kidd Creek mine is similar to other mines in Northern Ontario: horizontal stresses are greater than the vertical stress. In the horizontal plane, the magnitude of the principal stresses are almost the same which implies that the orientation of the openings is not critical in respect to stress direction. In most cases vertical stress is equivalent to the overburden pressure, whereas average horizontal stress, σh, can be related to depth, H, by:

$$\sigma h = 8.00 + 0.041\ H \text{ in MPa}$$

Deformation measurements around the first underground stope indicate that the expansion of the footwall shear zone into the stope is an order of magnitude greater centimetres compared with millimetres - than the pillar wall. There is a distinct cause-and-effect relationship between blasting and deformation and it is mainly mining on the same horizon that has the major effect, which suggests that deformation is related to lateral stope span. Broken ore in the stope seems to provide constraints to the footwall shear zone. When the broken ore is drawn down there is an accelerated displacement of the shear zone. Backfilling the stope with cemented rockfill also caused a slight reverse movement of the shear zone.

Only a preliminary analysis could be done on pillar stability as size of the pillars and the complex loading history are beyond present knowledge and experience. For pillars on the 1200 level, the analysis suggested that stresses on the pillar edges and corners could be of the same magnitude as pillar strength i.e., 46 to 54 MPa. This could explain the cases of pillar sloughing; alternatively, adverse structural geology could also have caused this sloughing.

Pillar stability could be improved by reducing the exposed length, which for long stopes, could be achieved by mining it in two sections with backfilling of the first section prior to mining the second. Another method would be to arrange the extraction sequence so that an ore or backfill pillar is never exposed on both sides simultaneously. This can be accomplished using a 5-unit block sequence.

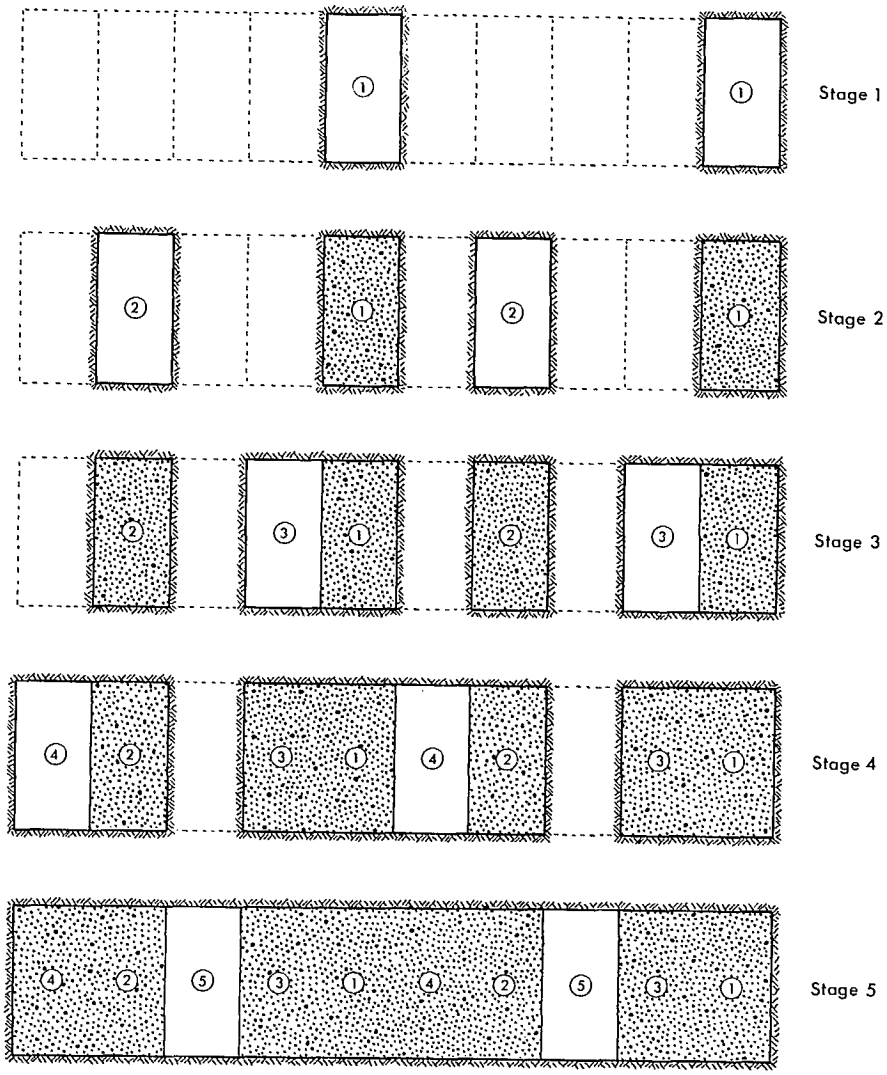

Fig. 4.10 - A five unit sequence of extraction.

ACKNOWLEDGEMENTS

The authors would like to thank B.A. Thomson, vice-president and general manager and J.E. Belford, manager of mines of the Kidd Creek operations of Texasgulf Canada Limited for actively encouraging this joint project. At the mine, T. Dowe, senior planning engineer, W. Totten, chief surveyor, T.R. Yu, rock mechanics engineer, and A. Matulich, chief geologist provided information and arranged the installation of measuring equipment and subsequent monitoring. Finally, O. Vaclavek and R. Wheeler painstakingly took most of the surveying and extensometer measurements.

Within the Mining Research Laboratories, N. Toews provided advice on the finite element models and W. Zawadski and L. Tirrul assisted with measurements and testing.

REFERENCES

1. Walker, R.R., Matulich, A., Amos, A.C., Watkins, J.J. and Mannard, G.W. "The geology of the Kidd Creek mine"; Economic Geology; vol 70; 1975.

2. Coupland, G.C. "The Ecstall story: the open-pit mine"; Can Min Metall Bull; May 1974.

3. Thomson, B.A., Blakey, P.N. and Paquette, J.P. "The Ecstall story: the transition from pit to underground"; Can Min Metall Bull; May 1974.

4. Belford, J.E., Amyotte, C.V., Edwards, F.A. and Ramsay, J. "The Ecstall story: the underground mine"; Can Min Metall Bull; May 1974.

5. Coates, D.F. "Pit slope manual, chapter 5 - design"; CANMET Report 77-5; CANMET, Energy, Mines and Resources Canada; Mar 1977.

6. Herget, G. "Pit slope manual supplement 2-4 joint mapping by terrestrial photogrammetry"; CANMET Report 77-23; CANMET, Energy, Mines and Resources Canada; 1977.

7. Hoek, E. and Bray, J.W. "Rock slope engineering"; Institute of Mining and Metallurgy, London; 1974.

8. Hoek, E. "Brittle failure of rock"; chapter 4 of "Rock mechanics in engineering practice"; (Ed.) Stagg, K. and Zienkiewicz, O.C.; John Wiley and Sons; p 442; 1968.

9. McMahon, B.K. "A statistical method for design of rock slopes"; Proc 1st Australia and New Zealand Conf Geomech; 1:314-321; 1971.

10. Herget, G. "Analysis of discontinuity orientation for a probabilistic slope stability design"; 19th U.S. Rock Mech Symp; 1978.

11. Deere, D.V. "Technical description of rock cores for engineering purposes"; Rock Mechanics and Engineering Geology; 1:1; 1964.

12. Wang, F.D., Sun, M.C. and Ropchan, D.M. "Computer program for pit slope stability analysis by the finite element stress analysis and limiting equilibrium method"; Report of Investigations 7685; USBM; 1972.

13. Herget, G. "Variation of rock stresses with depth at a Canadian iron mine"; Int J Rock Mech and Min Sci, 10:1; 1973.

14. Salamon, M.D.G., and Munro, A.H. "A study of the strength of coal pillars; J. S Afr Inst Min Met; Sept 1967.

15. Hedley, D.G.F. and Grant, F. "Stope-and-pillar design for the Elliot Lake uranium mines"; CIM Bull; July 1972.

16. Obert, L. and Duvall, W.I. "Rock mechanics and design of structures in rock"; New York; John Wiley; 1967.

APPENDIX A

OPEN PIT MONITORING SYSTEM AT THE KIDD CREEK MINE

A number of surveying methods exist for measuring the three-dimensional coordinates of a point. Triangulation involves measuring angles from two base stations of known coordinates to the target. Trilateration is a similar method except that only distances are measured. Traversing involves measuring both angles and distance from one instrument station to the target plus the horizontal angle to a known reference point.

At the Kidd Creek mine there was only one location on the west ramp with clear lines of sight to the whole southeast pit wall, hence a traversing system was chosen. Also measurements with this method are less time-consuming than triangulation or trilateration. In 1973 there were only a few instruments on the market capable of measuring both distance and angles, compared with those commercially available in 1978. After comparing instrument specifications and limited field trials a Geodimeter 700 was chosen. The specifications for the instrument are as follows:

Range:	1700 m with 1 glass prism
	3500 m with 3 glass prisms
	5000 m with 6 glass prisms
Resolution:	1 mm
Accuracy:	±5 mm + 1 mm/km mean square error
Light source:	1 mW HeNe gas laser
Horizontal angle:	2 s mean pointing accuracy
Vertical angle:	3 s mean pointing accuracy
Power supply:	12 V battery
Temperature range:	-30°C to +50°C
Readout:	7-digit "Numitron" tube

As all the measuring distances were within 1700 m, a single glass-prism reflector could be used for all targets.

Figure A.1 shows the construction details of the instrument stations and the two types of targets used. To obtain clear lines of sight to the southeast pit wall, the west ramp station had to be located at the edge of the pit in fractured ground. Rock bolts were installed and a cement-filled steel drum placed around the bolts as shown in Fig. A.1(a) in efforts to achieve the most stable station possible for the conditions. At a later date a cement pad was poured but not in contact with the steel pipe and a hut was constructed around the station. Outcrop East and Outcrop South Station are of similar construction except they were bolted to solid rock.

Along the haulage ramps and pit crest there was continual access and a detachable target, as shown in Fig. A.1(b), was moved from station to station. Along the pit berms was very limited access and permanent targets were cemented to the rock face as shown in Fig. A.1(c). The permanent targets are inside a steel casing to protect the glass-prism from small pieces of falling rock. Some of the detachable targets along the east ramp were damaged by snow ploughing and were replaced by permanent targets. Reject glass prisms, either damaged or sub-standard, were used on some of the permanent targets and gave acceptable measurements over sighting distances of 300 m. Trials were made with small plastic reflectors but soon after installation accumulations of dust prevented adequate return signals of the laser beam.

The measurement procedure and method of correcting for atmospheric conditions are as follows using the targets on the southeast pit wall as an example:

a. The Geodimeter 700 is mounted on top of the steel pipe of the West Ramp Station, which has forced centring (Fig. A.1(a)). The readout unit and a 12-volt car battery are connected and the instrument calibrated following the manufacturer's procedure.
b. Outcrop East Station is used as the backsight and the horizontal angles to all targets are relative to this station. The slope distance between the West Ramp Station and Outcrop East Station is used as a baseline and as a means of correcting for changes in temperature and air pressure. On the first set of readings in June 1973 the mean slope distance to Outcrop East was 441.473 m. In all subsequent sets of measurement Outcrop East is sighted and the distance reading is made to be 441.473 m by adjusting the atmospheric correction dial on the instrument. Hence the distances to all other targets are automatically corrected for atmospheric conditions,

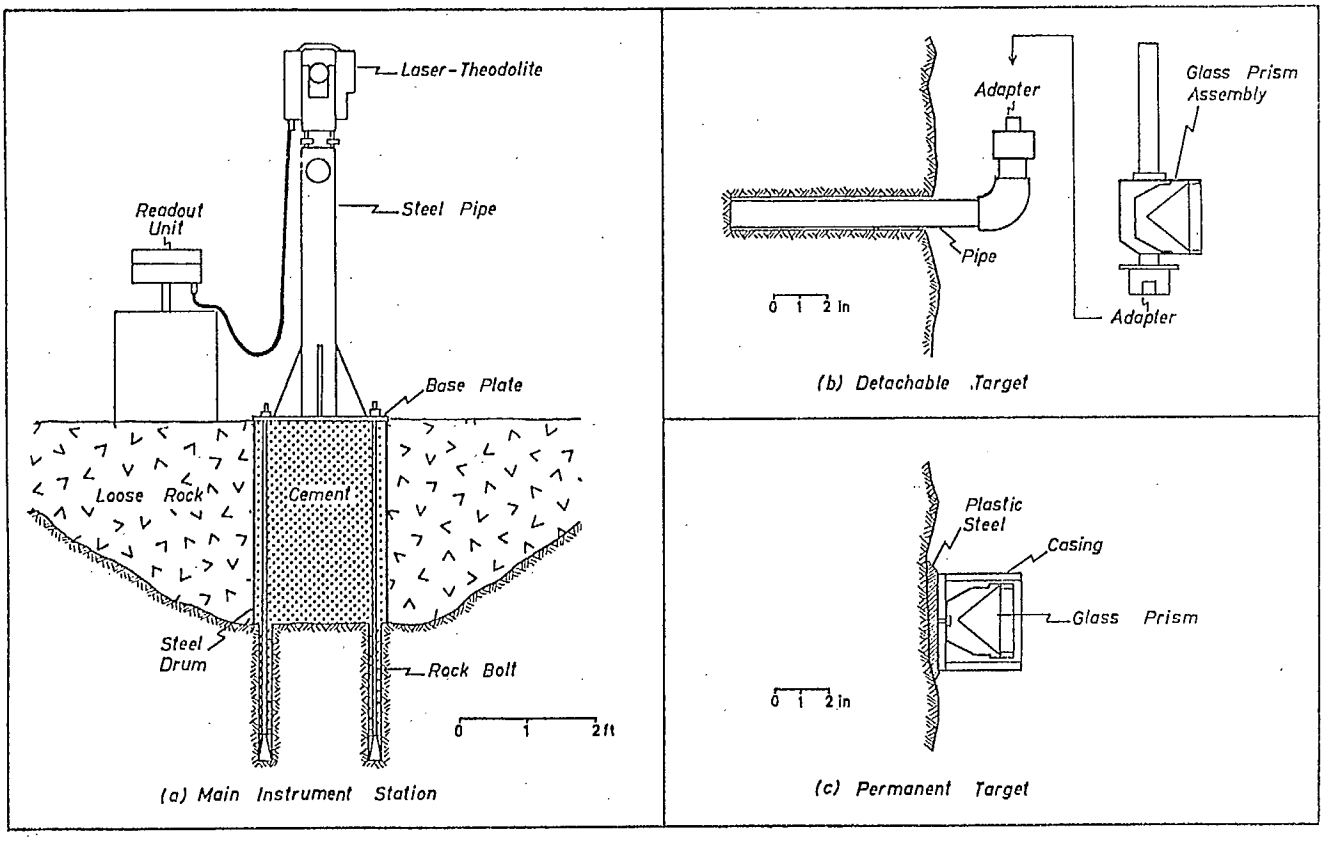

Fig. A-1 - Construction details of instrument station and targets.

provided neither of the stations move as explained later.

c. The 30 targets on the southeast wall are divided into sets of 5. Readings of slope distance, horizontal angle and vertical angle are taken to each target in turn, starting with Outcrop East Station. The telescope is then reversed and the same readings are repeated ending at Outcrop East Station. This procedure takes about half an hour for each set of 5 targets and prevents losing all the readings if the instrument is accidentally knocked.

d. This procedure is repeated for the other sets of targets. In the initial two years the whole process was repeated so that four individual measurements were made for each target. As experience was gained and consistency of the readings improved, only two measurements were made for each target and if there were a large discrepancy a check would be made the following week.

e. The readings of slope distance, horizontal and vertical angles to each target are averaged and these values are used to calculate the 3-D coordinates.

After the first year of measurement, it became obvious that the West Ramp Station was moving. This movement can be calculated if it is assumed that the Outcrop East and Outcrop South Stations have remained stable. Figure A.2 shows the diagramatic layout of the instrument and reference stations and lists the original measurements taken in 1973 and those in 1978.

In the measuring procedure the slope distance between the West Ramp and Outcrop East Stations is always made to be 441.473 m. As the West Ramp Station has moved, this distance is no longer correct and it is necessary to calculate the actual horizontal distance between the West

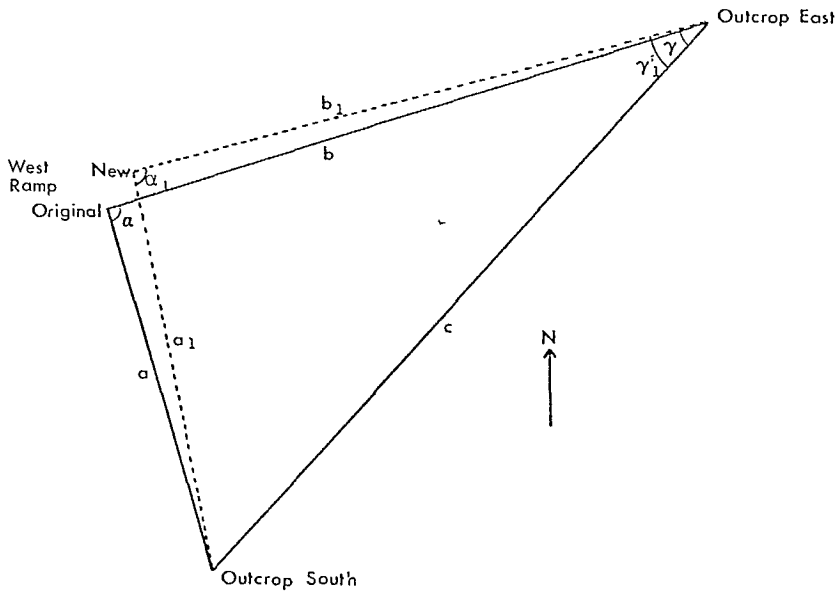

	Measurements 1973	1978
Slope distance, West Ramp to Outcrop East	m = 441.473 m	m_1 = 441.473
Vertical angle, West Ramp to Outcrop East	υ = +3°24'44"	υ_1 = +3°24'47"
Horizontal distance, West Ramp to Outcrop East	b = 440.690	b_1
Slope distance, West Ramp to Outcrop South	n = 266.688 m	n_1 = 266.727 m
Vertical angle, West Ramp to Outcrop South	ϕ = +2°11'05"	ϕ = +2°11'05"
Horizontal distance, West Ramp to Outcrop South	a = 266.495 m	a_1
Horizontal angle, Outcrop East, West Ramp, Outcrop South	α = 92°30'15"	α_1 = 92°30'32"
Horizontal distance, Outcrop East to Outcrop South	C = 524.870 m	

Fig. A-2 - Method of calculating movement of West Ramp Station.

Ramp Station and Outcrop East (b_1) and Outcrop South (a_1). The ratio of the measured slope distance is correct and can be expressed as:

$$\frac{m_1}{n_1} = \frac{441.473}{266.727} = 1.65515$$

$$\text{or } m_1 = 1.65515\ n_1 \qquad \text{Eq A1}$$

The horizontal distances can be expressed by:

$$b_1 = m_1 \cos \theta_1 \qquad \text{Eq A2}$$

and $$a_1 = n_1 \cos \phi_1 \qquad \text{Eq A3}$$

Substituting the values of θ_1 and ϕ_1 in Eq A2 and A3 and incorporating into Eq A1 gives:

$$b_1 = 1.65342\ a_1 \qquad \text{Eq A4}$$

Also, $c^2 = a_1^2 + b_1^2 - 2a_1b_1 \cos \alpha_1$ Eq A5

From equations A4 and A5 a_1 and b_1 can be calculated:

$a_1 = 266.512$ m and $b_1 = 440.656$ m

From the original distances a and b and the current distances a1 and b1 angles α and $\alpha 1$ can be calculated using the basic equation:

$$\cos \alpha = \frac{b^2 + c^2 - a^2}{2bc} \quad \text{Eq A6}$$

which gives, $\alpha = 30° 28' 51"$ and $\alpha_1 = 30° 28' 58"$. This 7-s increase in angle means that the angle from Outcrop East, Ramp West and Grid East has decreased by 7-s. The original angle of Grid East was 16° 59' 49" and hence the new Grid East angle is 16° 59' 42".

Using the original and new angles of grid east and the respective horizontal distances b and b_1, the northing and easting coordinates can be calculated for the West Ramp Station:

	Original	New	Change
Northing	-128.823 m	-128.799	+0.024 m
Easting	-421.441 m	-421.413	+0.028 m

Consequently, the West Ramp Station has moved in a northeasterly direction towards the pit. The total movement in the horizontal plane can be calculated from:

$$\sqrt{24^2 + 28^2} = 37 \text{ mm.}$$

The West Ramp, Outcrop East and Outcrop South Stations are periodically surveyed by triangulation, the last time being June 1978. This survey showed that the West Ramp Station had moved 0.027 m to the north and 0.024 m to the east. These values are very close to those calculated above.

The change in elevation of the West Ramp Station can be calculated from the general equation:

$$\text{Elevation} = b \tan \theta \quad \text{Eq A7}$$

Inserting the relevant values gives the original elevation as - 26.276 m and the new elevation as - 26.281 m indicating a downward movement of the West Ramp Station of 5 mm.

The procedure for calculating the coordinates of the targets is as follows:

1. The slope distance to each target is corrected by multiplying by

$$\frac{m^1 \, n}{n^1 \, m}$$

2. The coordinates of each target are calculated using the new grid east angle and related to the new position of the West Ramp Station.
3. These coordinates are then corrected for the movement of the West Ramp Station so that they are related to the original coordinate system.

CANMET REPORTS

Recent CANMET reports presently available or soon to be released through Printing and Publishing, Supply and Services, Canada (addresses on inside front cover), or from CANMET Publications Office, 555 Booth Street, Ottawa, Ontario, K1A 0G1:

Les récents rapports de CANMET, qui sont présentement disponibles ou qui ce seront bientôt peuvent être obtenus de la direction de l'Imprimerie et de l'Edition, Approvisionnements et Services, Canada (adresses au verso de la page couverture), ou du Bureau de Vente et distribution de CANMET, 555 rue Booth, Ottawa, Ontario, K1A 0G1:

79-1 Tantalum and niobium ore dressing investigations at CANMET; D. Raicevic and H.L. Noblitt;
Cat. No. M38-13/79-1, ISBN 0-660-10419-9; Price: $3.85 Canada, $4.65 other countries.

79-2 Synthesis and characterization of zirconia electrolytes for potential use in energy conversion systems; T.A. Wheat;
Cat. No. M38-13/79-2, ISBN 0-660-10405-9; Price: $1.75 Canada, $2.10 other countries.

79-6 Heat-affected-zone toughness of welded joints in micro-alloy steels; (Noranda Research) D.W.G. White and K. Winterton, editors;
Cat. No. M38-13/79-6, ISBN 0-660-10413-X; Price: $5.75 Canada, $6.90 other countries.

79-9 Construction and operation of a continuous ion exchange pilot plant using fluidized-bed columns; P. Prud'homme and B.H. Lucas;
Cat. No. M38-13/79-9, ISBN 0-660-10440-7; Price: $1.25 Canada, $1.50 other countries.

79-13 Liquid fuels from Canadian coals; G. Taylor;
Cat. No. M38-13/79-13, ISBN 0-660-10424-5; Price: $3.10 Canada, $3.75 other countries.

79-14 Zinc concentrate CZN-1 - A certified reference material; G.H. Faye, W.S. Bowman and R. Sutarno;
Cat. No. M38-13/79-14, ISBN 0-660-10270-6; Price: $2.00 Canada, $2.40 other countries.

79-15 Lead concentrate CPB-1 - A certified reference material; G.H. Faye, W.S. Bowman and R. Sutarno;
Cat. No. M38-13/79-15, ISBN 0-660-10287-0; Price: $2.00 Canada, $2.40 other countries.

79-16 Copper concentrate CCU-1 - A certified reference material; G.H. Faye, W.S. Bowman and R. Sutarno;
Cat. No. M38-13/79-16, ISBN 0-660-10288-9; Price $1.45 Canada, $1.75 other countries.

79-19 Test installation for studying erosion-corrosion of metals for coal washing plants; G.R. Hoey, W. Dingley and C.T. Wiles;
Cat. No. M38-13/79-19, ISBN 0-660-10420-2; Price: $1.10 Canada, $1.35 other countries.

79-21 Removal of radionuclides from process streams - A survey; I.J. Itzkovitch and G.M. Ritcey;
Cat. No. M38-13/79-21, ISBN 0-660-10409-1; Price: $8.00 Canada, $9.60 other countries.

79-22 Mineral waste resources of Canada report no. 3 - Mining wastes in British Columbia; R.K. Collings;
Cat. No. M38-13/79-22, ISBN 0-660-10407-5; Price: $2.00 Canada, $2.40 other countries.

79-24 A study and assessment of the technological capabilities of the Canadian foundry industry; (R. Shnay and Associates Ltd.) R.K. Buhr, editor;
Cat. No. M38-13/79-24, ISBN 0-660-10427-X; Price: $3.25 Canada, $3.90 other countries.

79-27 Mineralogy of samples from the Lac des Iles area, Ontario; L.J. Cabri and J.H.G. Laflamme;
Cat. No. M38-13/79-27, ISBN 0-660-104030-X; Price: $1.00 Canada, $1.20 other countries.